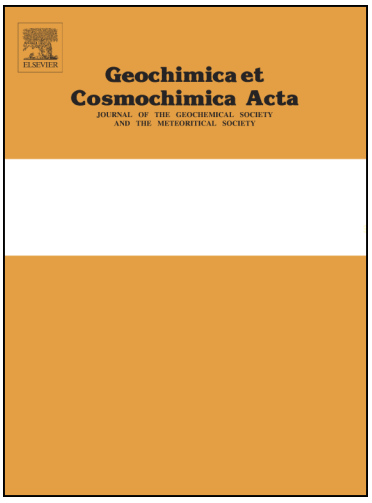

A Model for the Oceanic Mass Balance of Rhenium and Implications for the Extent of Proterozoic Ocean Anoxia

Alex I. Sheen, Brian Kendall, Christopher T. Reinhard, Robert A. Creaser, Timothy W. Lyons, Andrey Bekker, Simon W. Poulton, Ariel D. Anbar

PII: S0016-7037(18)30066-8
DOI: https://doi.org/10.1016/j.gca.2018.01.036
Reference: GCA 10639

To appear in: *Geochimica et Cosmochimica Acta*

Received Date: 13 July 2017
Accepted Date: 30 January 2018

Please cite this article as: Sheen, A.I., Kendall, B., Reinhard, C.T., Creaser, R.A., Lyons, T.W., Bekker, A., Poulton, S.W., Anbar, A.D., A Model for the Oceanic Mass Balance of Rhenium and Implications for the Extent of Proterozoic Ocean Anoxia, *Geochimica et Cosmochimica Acta* (2018), doi: https://doi.org/10.1016/j.gca.2018.01.036

A Model for the Oceanic Mass Balance of Rhenium and Implications for the Extent of Proterozoic Ocean Anoxia

Alex I. Sheen[a,b], Brian Kendall[a], Christopher T. Reinhard[c], Robert A. Creaser[b], Timothy W. Lyons[d], Andrey Bekker[d], Simon W. Poulton[e], Ariel D. Anbar[f,g]

[a] Department of Earth and Environmental Sciences, University of Waterloo, 200 University Avenue West, Waterloo, Ontario, Canada N2L 3G1

[b] Department of Earth and Atmospheric Sciences, University of Alberta, Edmonton, Alberta T6G 2E3, Canada

[c] School of Earth and Atmospheric Sciences, Georgia Institute of Technology, Atlanta, Georgia 30332, USA.

[d] Department of Earth Sciences, University of California, Riverside, CA 92521, USA

[e] School of Earth and Environment, University of Leeds, Leeds LS2 9JT, UK

[f] School of Earth and Space Exploration, Arizona State University, Tempe, AZ 85287, USA

[g] School of Molecular Sciences, Arizona State University, Tempe, AZ 85287, USA

Revision submitted to: Geochimica et Cosmochimica Acta

January 19, 2018

*Corresponding author at: Department of Earth and Atmospheric Sciences, University of Alberta, Edmonton, Alberta T6G 2E3, Canada. Email: asheen@ualberta.ca.

Abstract

Emerging geochemical evidence suggests that the atmosphere-ocean system underwent a significant decrease in O_2 content following the Great Oxidation Event (GOE), leading to a mid-Proterozoic ocean (ca. 2.0–0.8 Ga) with oxygenated surface waters and predominantly anoxic deep waters. The extent of mid-Proterozoic seafloor anoxia has been recently estimated using mass-balance models based on molybdenum (Mo), uranium (U), and chromium (Cr) enrichments in organic-rich mudrocks (ORM). Here, we use a temporal compilation of concentrations for the redox-sensitive trace metal rhenium (Re) in ORM to provide an independent constraint on the global extent of mid-Proterozoic ocean anoxia and as a tool for more generally exploring how the marine geochemical cycle of Re has changed through time. The compilation reveals that mid-Proterozoic ORM are dominated by low Re concentrations that overall are only mildly higher than those of Archean ORM and significantly lower than many ORM deposited during the ca. 2.22–2.06 Ga Lomagundi Event and during the Phanerozoic Eon. These temporal trends are consistent with a decrease in the oceanic Re inventory in response to an expansion of anoxia after an interval of increased oxygenation during the Lomagundi Event. Mass-balance modeling of the marine Re geochemical cycle indicates that the mid-Proterozoic ORM with low Re enrichments are consistent with extensive seafloor anoxia. Beyond this agreement, these new data bring added value because Re, like the other metals, responds generally to low-oxygen conditions but has its own distinct sensitivity to the varying environmental controls. Thus, we can broaden our capacity to infer nuanced spatiotemporal patterns in ancient redox landscapes. For example, despite the still small number of data, some mid-Proterozoic ORM units have higher Re enrichments that may reflect a larger oceanic Re inventory during transient episodes of ocean oxygenation. An improved understanding of the modern oceanic Re cycle and a higher

temporal resolution for the Re compilation will enable further tests of these hypotheses regarding changes in the surficial Re geochemical cycle in response to variations in atmosphere-ocean oxygenation. Nevertheless, the existing Re compilation and model results are in agreement with previous Cr, Mo, and U evidence for pervasively anoxic and ferruginous conditions in mid-Proterozoic oceans.

Keywords: rhenium; anoxia; Proterozoic; organic-rich mudrocks; ocean; oxygen

1. Introduction

The progressive oxygenation of the early Earth's surface had a profound impact on Earth's biological and geochemical evolution (Lyons et al., 2014). A poorly oxygenated atmosphere-ocean system in the Archean is indicated by several lines of evidence in the sedimentary record (Farquhar et al., 2000; Bekker et al., 2010; Sverjensky and Lee, 2010; Lyons et al., 2014), such as abundant banded iron formations (BIF), common occurrence of redox-sensitive detrital minerals, and preservation of sulfur mass-independent fractionation (S-MIF). In addition, the low concentrations of some redox-sensitive elements (e.g., Mo, U) in sedimentary archives suggest low seawater concentrations of these elements because of their limited oxidative mobilization from the Archean continental crust (Scott et al., 2008; Partin et al., 2013). The Great Oxidation Event (GOE) is marked by a permanent increase of atmospheric O_2 content to >0.001% present atmospheric level (PAL), starting between 2.45 and 2.32 Ga (Pavlov and Kasting, 2002; Bekker et al., 2004; Bekker, 2014; Gumsley et al., 2017). This transition was accompanied by the appearance of new mineral species containing redox-sensitive elements in their highest oxidation states, reduction in BIF deposition, disappearance of S-MIF, and an increase in seawater Mo, U, and sulfate concentrations (Bekker et al., 2004, 2010, 2013; Schröder et al., 2008; Scott et al., 2008, 2014; Sverjensky and Lee, 2010; Hazen et al., 2011; Planavsky et al., 2012; Reuschel et al., 2012; Partin et al., 2013; Reinhard et al., 2013a). The latter part of the GOE was marked by a protracted episode of elevated organic carbon burial (Lomagundi Event) between ca. 2.22 and 2.06 Ga, which suggests a long-lasting, but transient increase in atmosphere-ocean O_2 contents to levels that may not have occurred again until the Neoproterozoic Oxidation Event (NOE) (Karhu and Holland, 1996; Scott et al., 2008, 2014; Kump et al., 2011; Planavsky et al., 2011, 2012, 2014; Bekker and Holland, 2012; Partin et al., 2013).

Although dramatic swings in the extent of atmosphere-ocean oxygenation are recognized in the early and late Proterozoic, surficial redox dynamics during the intervening period were likely muted. Recent geochemical data (e.g., redox-sensitive trace metals and Fe speciation) suggest stratified ocean redox conditions for the middle portion of the Proterozoic (ca. 1.8–0.8 Ga; hereafter referred to as the mid-Proterozoic), wherein oxygenated surface waters were underlain by euxinic (anoxic and sulfidic) waters in highly productive marginal settings, and ferrous iron (Fe^{2+}) accumulated in suboxic to anoxic deep waters in offshore settings (ferruginous anoxia; Poulton et al., 2010; Planavsky et al., 2011; Reinhard et al., 2013a; Sperling et al., 2015). While Fe speciation data indicate ferruginous conditions at many times and localities in the mid-Proterozoic, the scarcity of preserved ancient seafloor, particularly of the deepest parts of the ocean, creates a challenge for constraining the marine redox landscape on a global scale.

Although low O_2 levels have been suggested for the mid-Proterozoic atmosphere–ocean system (<0.1–1.0% PAL; Canfield, 1998; Reinhard et al., 2013a; Planavsky et al., 2014; Liu et al., 2016; Tang et al., 2016; Hardisty et al., 2017), such conditions imply poorly buffered surface O_2 inventories and the potential for significant spatiotemporal variability (Planavsky et al., 2014; Cole et al., 2016; Reinhard et al., 2016; Daines et al., 2017; Hardisty et al., 2017). Indeed, there has been much recent interest in the possibility of dynamic spatiotemporal variations in atmosphere-ocean redox conditions during this time (e.g., Sperling et al., 2014; Gilleaudeau and Kah, 2015; Gilleaudeau et al., 2016; Mukherjee and Large, 2016; Planavsky et al., 2016; Reinhard et al., 2016; Zhang et al., 2016) against a background of lower atmospheric pO_2 compared with today (e.g., Cole et al., 2016). Hence, additional data and proxies sensitive to global redox conditions are needed to better understand the spatiotemporal evolution and the dominant redox state of the mid-Proterozoic oceans. Such information is critical to a full

understanding of the relationship between Earth's surface oxygenation and the evolution of both eukaryotic organisms and complex metazoan life. The integrated use of diverse metals spanning a broad range of redox sensitivity (e.g., Reinhard et al., 2013a), detrital backgrounds, uptake pathways, and crustal sources will strengthen our conclusions.

The concentrations of some redox-sensitive trace metals in marine organic-rich mudrocks (ORM) can provide insight into global ocean redox conditions. Behaving largely conservatively in oxygenated seawater, trace metals such as Mo, Cr, Re, and U are removed to anoxic sediments at higher rates compared with oxygenated sediments, with removal rates dependent on the specific chemistry of the water column and underlying sediment pore fluids (e.g., Morford and Emerson, 1999; Tribovillard et al., 2006). Chromium, U, and Re become authigenically enriched in sediments overlain by an anoxic water column (at both high and low levels of dissolved H_2S) and, to a lesser extent, in anoxic sediments overlain by mildly oxygenated bottom waters (Crusius et al., 1996; Morford and Emerson, 1999; Morford et al., 2005; Partin et al., 2013; Reinhard et al., 2013a). By contrast, high authigenic Mo enrichments in sediments require the accumulation of dissolved H_2S in the water column. Anoxic sediments beneath mildly oxygenated bottom waters display mild Mo enrichments if dissolved H_2S is present in sediment pore fluids at shallow depths below the sediment-water interface (Crusius et al., 1996; Morford and Emerson, 1999; Morford et al., 2005).

Because these trace metals have a long seawater residence time relative to the average ocean turnover time (~1–2 kyr), their enrichment record in open-marine anoxic sediments reflects, in principle, the global marine redox state. Once an environment becomes authigenically active for a particular redox-sensitive trace metal, the degree of authigenic enrichment of that metal in sediments will be broadly proportional to its dissolved seawater inventory (Algeo and Lyons,

2006; Scott et al., 2008; Reinhard et al., 2013a). On a global scale, that inventory will be controlled mainly by the collective state of marine redox conditions—once pervasive oxidative continental weathering and the associated riverine flux of dissolved anionic metal complexes are established (Scott et al., 2008; Partin et al., 2013; Reinhard et al., 2013a). In an ancient ocean that was more anoxic than today, a globally higher rate of metal burial in seafloor sediments should occur, leading to a decrease in seawater metal concentrations and thus lower metal enrichments in coeval ORM (Scott et al., 2008; Sahoo et al., 2012; Partin et al., 2013; Reinhard et al., 2013a).

Building from the approach of Scott et al. (2008), new constraints on the extent of ocean anoxia were recently presented for the mid-Proterozoic ocean using trace element records. Through a mass-balance model combined with Mo and Cr enrichments in ORM, Reinhard et al. (2013a) estimated the extent of mid-Proterozoic anoxia to be at least 30–40% of the modern seafloor area, with euxinic conditions covering less than ~1–10% of the modern seafloor. In fact, the Cr enrichment record is also consistent with virtually complete seafloor anoxia. A disadvantage of Cr, however, is its high detrital contribution to ORM (Reinhard et al., 2013a), which makes it an intrinsically less precise tracer for the benthic redox landscape under conditions of pervasive marine anoxia. Based on the U record, Partin et al. (2013) postulated that anoxic conditions covered over 50% of the modern seafloor area. However, this estimate assumes that the U burial flux in anoxic basins on continental margins applies to the global seafloor. Hence, the mass-balance model of Partin et al. (2013) is over-sensitive to anoxic conditions and consequently may underestimate the true extent of ocean anoxia.

Rhenium (Re) behaves conservatively in oxygenated seawater and, unlike Mo, can be efficiently removed to anoxic sediments at low dissolved H_2S levels when the bottom waters are

weakly oxygenated or anoxic, thus making it a more effective proxy for tracking general ocean anoxia (i.e., combined euxinic and ferruginous anoxia) (Colodner et al., 1993; Crusius et al., 1996; Morford and Emerson, 1999; Morford et al., 2005, 2012). Although Cr and U behave similarly in this regard (Partin et al., 2013; Reinhard et al., 2013a), the magnitude of authigenic Re enrichment in anoxic marine sediments is significantly higher than the detrital background compared with Cr and U, as reflected by higher Re enrichment factors in organic-rich sediments expressed relative to average upper crust (Table 1). These higher Re enrichments indicate that Re is more sensitive to O_2-deficient conditions than Cr and U and can potentially provide more quantitatively precise information on deep-sea redox state. Because of these distinct geochemical properties, the enrichment record of Re in anoxic marine ORM may provide a novel and complementary perspective on global ocean redox conditions.

To estimate first-order variations in the seawater concentration of Re through geologic time, with new insights into the evolution of marine redox conditions during the mid-Proterozoic as the primary goal, we compiled Re concentration data for ORM from the literature and report new Re concentration data from several Precambrian intervals. We quantify the sources and sinks of the Re marine cycle based on modern observations and integrate these observations with the mass-balance approach developed by Reinhard et al. (2013a). Using this mass-balance model, we discuss the sensitivity of the marine Re cycle with respect to the expansion and contraction of ocean anoxia during this interval of Earth's history and its implications for the extent and variability of mid-Proterozoic ocean anoxia.

2. The modern marine Re cycle

2.1 Marine sources

Rhenium exists in seawater primarily as the soluble perrhenate oxyanion ReO_4^-, with a concentration of 40 pmol kg^{-1} (Anbar et al., 1992; Colodner et al., 1993). In the modern ocean, most of this dissolved reservoir is derived from oxidative weathering of sulfide minerals, based on the good correlation observed globally between Re and sulfate concentrations in rivers, and from weathering of ORM in the upper continental crust (Colodner et al., 1993; Miller et al., 2011; Dubin and Peucker-Ehrenbrink, 2015). Excluding anthropogenic inputs, the average Re concentration of rivers has been calculated to be 11.2 pmol kg^{-1} based on data from 38 rivers on five continents (~37% of total water discharge; 25% of continental exorheic drainage area). This estimate yields a riverine flux of 4.29×10^5 mol yr^{-1}, which corresponds to a seawater residence time of 1.3×10^5 yr (Miller et al., 2011).

Seafloor hydrothermal vents have been considered as an additional component of the marine Re cycle (Morford and Emerson, 1999). It is postulated that Cl^- complexation in high-temperature hydrothermal fluids may yield high Re concentrations (Xiong and Wood, 1999; 2002). However, Re may be removed from such fluids by precipitation of sulfides under fluid-sulfide equilibrium (Miller et al., 2011). Miller et al. (2011) presented the first published Re measurements in high-temperature hydrothermal fluids in the Manus Basin, and estimated a flux of 1.2×10^3 mol yr^{-1} from these data. If globally representative, this flux constitutes 0.1% of the pre-anthropogenic riverine Re input and thus has a negligible influence on the modern oceanic Re mass balance.

Low-temperature hydrothermal fluids are a possible minor source of Re to the modern ocean (as is the case for Mo; Morford and Emerson, 1999), but no data exist to quantify this flux. Reinhard et al. (2013a) calculated that the modern low- and high-temperature hydrothermal

fluxes of Mo and Cr are unlikely to be above ~10% and ~1% of their riverine fluxes, respectively. Given the similar geochemical behaviour of Re and Mo, it is reasonable to assume that the modern hydrothermal flux of Re to the oceans is also small.

2.2 Marine Sinks

2.2.1 Overview

Sinks for Re removal from modern seawater comprise sediment burial in three redox settings: oxic, suboxic (defined below), and anoxic. Because of the solubility of ReO_4^-, Re accumulation is typically very slow in well-oxygenated marine settings where O_2 penetrates more than 1 cm below the sediment-water interface. By contrast, Re accumulation is significantly more efficient in anoxic marine settings. Rhenium removal from an anoxic water column is likely dominated by abiotic redox reactions rather than biological uptake. In anoxic conditions, Re is reduced from the soluble heptavalent (VII) to the insoluble tetravalent (IV) state (Colodner et al., 1993; Crusius et al., 1996; Morford and Emerson, 1999; Morford et al., 2005). Scavenging of Re^{4+} by organic matter is suggested by the direct association of Re with organic matter in fine-grained sediments and their lithified equivalents (ORM) (Selby and Creaser, 2003; Georgiev et al., 2012). In some ORM, a good positive correlation is observed between Re concentration and total organic carbon (TOC) content (e.g., Rooney et al., 2010) as has been observed for Mo (Algeo and Lyons, 2006), but this relationship is not observed in all ORM (e.g., Cohen et al., 1999). Decoupling of Re and TOC contents in ORM may reflect temporal (i.e., stratigraphic) variations in local bottom water Re concentrations at the site of deposition. Co-precipitation of Re^{7+} with a Fe–Mo–S phase has been proposed for the removal of

Re from sulfide-bearing waters (Helz and Dolor, 2012), which may also be responsible for a scatter of Re concentration versus TOC content in ORM.

Rhenium burial rates characteristic of each of the three settings are calculated based on observations in modern marine environments (Table 2; tables S1 and S2 in the supplementary database). Below, we describe how representative burial rates were calculated for each sink.

2.2.2 Oxic sink

Oxic settings are characterized by permanent burial of Mn oxides in sediments where O_2 penetration depths below the sediment-water interface are large. To be consistent with previous trace metal studies, we define oxic settings as those with an O_2 penetration depth >1 cm, at which point Mn redox cycling begins (Morford and Emerson, 1999). Rhenium adsorption onto Fe–Mn oxides is minimal relative to other redox-sensitive trace metals such as Mo (Koide et al., 1986; Colodner et al., 1993). As a reference frame, and as discussed in Reinhard et al. (2013a), the extent of modern seafloor covered by oxic sediments with an O_2 penetration depth >1 cm is ~84%.

The modern oxic Re sink is dominated by continental margin sediments, where the sediment mass accumulation rate is high. Previous Re budget reconstructions treat pelagic sediments, which form the majority of modern-day oxic seafloor, as a negligible sink. This assumption is supported by an average $[Re]_{sed}$ of 0.05 ppb in pelagic sediments of the North Atlantic (Colodner, 1991), which translates to a burial flux of 1.2×10^{-5} ng cm^{-2} yr^{-1} (assuming an average linear sedimentation rate). The pelagic burial rate in abyssal regions of the seafloor, when combined with an average burial rate of 7.4×10^{-3} ng cm^{-2} yr^{-1} for Re in shelf sediments deposited from well-oxygenated waters on continental margins (Sea of Japan, Central Arctic Ocean,

Northwestern US margin, and African margin; Table 2) yields an area-weighted average oxic Re burial rate of 1.6×10^{-3} ng cm^{-2} yr^{-1} (continental margin and deep-sea abyssal regions cover an area of 7.4×10^{17} cm^2 and 2.7×10^{18} cm^2, respectively; Sverdrup et al., 1942; Wollast, 2003). Again, the oxic burial rate is dominated by continental margin sediments and is unlikely to vary significantly with new estimates for pelagic sediments.

2.2.3 Suboxic sink

Similar to Mo, Cr, and U, a significant difference exists in Re accumulation rates beneath anoxic water columns and those under weakly oxygenated bottom waters (Colodner et al., 1993; Crusius et al., 1996; Morford and Emerson, 1999; Morford et al., 2005). To be consistent with previous studies on trace element redox modeling, we define the suboxic setting as areas where the O_2 penetration depth below the sediment-water interface is <1 cm (Partin et al., 2013; Reinhard et al., 2013a). This condition accounts for areas of the seafloor where dissolved O_2 is present in bottom waters, but typically at levels low enough (<10–100 μM; higher values are also possible in shallow coastal locations; Morford and Emerson, 1999; Morford et al., 2005, 2007, 2012) so that Fe–Mn oxyhydroxides are not permanently buried, and that reduction of Re occurs in the anoxic sediment pore-waters. The result is appreciable authigenic accumulation of Re in sediments. Beneath modern suboxic waters in continental margin environments, authigenic Re accumulation occurs without significant Mo accumulation when the shallow pore water is anoxic but dissolved H_2S is low, thus demonstrating that Re removal rate does not scale to H_2S availability (Morford and Emerson, 1999; Morford et al., 2005).

Depending on the organic carbon flux and oxygen penetration depth, modern suboxic Re burial rates range from 0.2–0.3 ng cm^{-2} yr^{-1} on the northwestern U.S. margin to ~1.5 ng cm^{-2} yr^{-1}

in the Gulf of California. Our estimate for the suboxic Re burial rate combines these values with those observed in oxygen-minimum zones and high productivity regions in the Californian Borderlands, African margin, Laurentian Trough, Buzzards Bay, Hingham Bay, and the Arabian Sea (Table 2). Weighting by relative areal extent yields a suboxic Re burial rate of 0.41 ng cm^{-2} yr^{-1}. The total area of modern suboxic seafloor is not precisely known and is solved using other sink parameters in the mass-balance model, following the methods of Reinhard et al. (2013a). Using this approach, the modern suboxic seafloor is calculated to make up ~4.7% of the global seafloor.

2.2.4 Anoxic sink

Rhenium is most effectively removed to sediments deposited from anoxic bottom waters. In the modern ocean, such environments are restricted to marginal basins (e.g., the Cariaco Basin), seafloors beneath areas of intense upwelling (e.g., the Peru margin and Namibian shelf), and highly restricted basins (e.g., the Black Sea). In the modern ocean, anoxic seafloor is dominated by euxinia defined as having an excess of sulfide relative to Fe (i.e., above a molar ratio of 1Fe:2S, the stoichiometric proportions of pyrite). During the Proterozoic Eon, however, ferruginous anoxia is believed to have been more widespread (Poulton et al., 2010; Planavsky et al., 2011). Extrapolating from modern observations that reveal significant authigenic Re accumulation without Mo accumulation in anoxic sediments when dissolved H_2S in pore waters is low, we infer that Re burial in sediments below anoxic waters does not depend on H_2S availability in the water column. This independence allows us to merge both types of anoxia into one sink in this study.

We adopt the latest estimate of ~0.11% for the modern anoxic seafloor area published by Reinhard et al. (2013a), which combines results from anoxic basin studies. A portion of modern anoxic settings is found in highly restricted basins where Re is significantly depleted in deep waters due to slow renewal rates (as demonstrated for the Black Sea; Colodner et al., 1995). As such, Re burial rates in restricted anoxic settings are lower compared with more open anoxic settings. For example, the estimated burial rate of Re in the Black Sea (<0.5 ng cm^{-2} yr^{-1}; Ravizza et al., 1991) is lower than those estimated for the less restricted Cariaco Basin (1.3–1.6 ng cm^{-2} yr^{-1}; Calvert et al, 2015; this study) and Saanich Inlet (1–1.5 ng cm^{-2} yr^{-1}; Poirier, 2006). For the purpose of establishing a model for the well-mixed open ocean, such highly restricted basins (e.g., the Black Sea) are excluded from our Re mass-balance.

Published measurements of anoxic Re burial rates exist for a few small basins such as Walvis Bay and Saanich Inlet (2.1 and 1–1.5 ng cm^{-2} yr^{-1}, respectively; Colodner et al., 1993; Poirier, 2006). Measurements from sediments beneath anoxic bottom waters along a few continental margins (characterized by intense upwelling) display much higher variation (Table 2). For our study, we prioritize new $[Re]_{sed}$ data from the large and well-characterized Cariaco Basin (see SI), which yield an anoxic burial rate of 1.34 ng cm^{-2} yr^{-1}, consistent with published values (Calvert et al., 2015; SI). The Cariaco Basin is the largest and best understood modern anoxic basin with a relatively unrestricted connection to the open ocean, as well as a fairly constant $[Re]_{sed}$ and a linear sedimentation rate (Peterson et al., 2000). Hence, we assume that this value is most representative of anoxic conditions in the modern ocean rather than assuming arithmetic or area-weighted averages of anoxic burial rates. In any case, the Re burial rate in the Cariaco Basin lies roughly in the middle of the range of Re burial rates observed in other unrestricted anoxic basins and upwelling continental margin systems.

Our estimated anoxic burial rate of ~1.34 ng cm^{-2} yr^{-1} is three times greater than the suboxic burial rate, averaged at 0.42 ng cm^{-2} yr^{-1}. The oxic burial rate, 1.6×10^{-3} ng cm^{-2} yr^{-1}, is extremely low by comparison. These averages are combined with the areal extent of each setting to determine the magnitude of the sink fluxes (Table 3). In summary, Re removal from modern seawater is dominated by the suboxic sink, which equates to 88% of the riverine flux. The oxic and anoxic sinks are much smaller, with both equating to ~6–7% of the riverine flux. This relationship is comparable with the modern Cr budget estimated by Reinhard et al. (2013a), where the oxic, suboxic, and anoxic sinks constitute 10%, 84%, and 6% of the riverine Cr flux, respectively. Again, the modern anoxic sink is relatively small despite efficient uptake because this redox condition is underrepresented in the modern ocean. The oxic, suboxic, and anoxic seafloor areas in our mass balance totals ~89% (Table 3; similar to Cr; Reinhard et al., 2013a), implying that ~11% of the seafloor is authigenically neutral with respect to Re (e.g. regions of the seafloor that do not remove Re from seawater).

Based on a redox-sensitive behavior of Re that is generally comparable to other redox-sensitive elements (e.g., Mo, Zn, and U), it is postulated that Re burial flux associated with the anoxic sink is controlled by the size of the dissolved Re reservoir; this is an important assumption in our study and remains to be confirmed and ideally quantified by experimental work and measurements of bottom-water Re concentrations from modern anoxic basins in addition to the data already available from the Black Sea. A significant implication of this assumption is that the size of the dissolved reservoir can be locally influenced by the degree of basin restriction from the open ocean. In the highly restricted Black Sea, for example, slow deep-water renewal rates have caused depletion of Re in the bottom waters (Colodner et al., 1995), which should cause lower Re enrichments and burial fluxes in organic-rich sediments (when

normalized to TOC) relative to less restricted anoxic settings. Indeed, the Re concentration and burial flux of Unit I sediments in the Black Sea are generally lower than those of the Cariaco Basin and other relatively open-ocean anoxic settings (Table 2; keeping in mind that sedimentation rate and organic carbon flux also locally influence Re concentrations in organic-rich sediments). A similar relationship between metal concentrations in bottom waters and organic-rich sediments in anoxic basins has been noted for other redox-sensitive elements (e.g., Mo, U, and Zn; Algeo and Lyons, 2006; Scott et al., 2008, 2013; Partin et al., 2013).

Extrapolating from this observation, the Re concentration of anoxic sediments deposited in relatively open-marine settings (i.e., negligible to mild basin restriction) should show a first-order relationship with the size of the global seawater Re reservoir, which in turn depends on the riverine flux and the temporally varying extent of oxic, suboxic, and anoxic conditions on the seafloor. The riverine flux of Re is assumed to have become largely independent of atmospheric O_2 levels at the early stage of the GOE, when atmospheric O_2 levels rose above the threshold (as low as <0.001% PAL) required to support subaerial oxidative dissolution of crustal sulfide minerals and delivery of the related products to the oceans (Hannah et al., 2004; Anbar et al., 2007; Reinhard et al., 2013b; Greber et al., 2015). Details of these assumptions await further study, particularly weathering relationships. However, changes in the size of the seawater Re inventory during the Proterozoic and Phanerozoic were likely controlled primarily by the global distribution of marine redox conditions. The first-order temporal and spatial extent of anoxic conditions in the mid-Proterozoic ocean can thus be inferred by examining the magnitude of Re enrichment in ORM.

3. Analytical methods

The pronounced enrichment of authigenic Re in anoxic ORM make this lithology the ideal archive for tracking changes in the oceanic Re reservoir through geological time. Hence, we compiled a database of Re concentrations and associated TOC contents in marine ORM through a literature survey, supplemented with new analyses of Precambrian ORM (see Supplementary database files). New Re concentration data were obtained via HF–HNO_3–HCl dissolution of ashed sample powders followed by analysis on a Thermo Scientific X Series quadrupole inductively coupled plasma mass spectrometer (Q–ICP–MS) at the W. M. Keck Foundation Laboratory for Environmental Biogeochemistry, Arizona State University, following the methods described in Anbar et al. (2007) and Kendall et al. (2010). Some new Re data were also obtained via Carius tube dissolution of sample powders in a Cr^{VI}–H_2SO_4 medium, chemical separation of Re, and analysis by isotope dilution–negative thermal ionization mass-spectrometry (ID–NTIMS; Thermo TRITON) at the Canadian Centre for Isotopic Microanalysis, University of Alberta (e.g., Kendall et al., 2015a). The accuracy of Re measurements by Q–ICP–MS was verified by analysis of ORM for which the Re concentrations were also determined by the more precise ID–NTIMS method (Kendall et al., 2010). Data reported in the literature were predominantly derived by ID–NTIMS and ICP–MS. Uncertainties for Re concentrations are usually <10% for Q–ICP–MS, and typically <1% for isotope dilution analysis using NTIMS or MC–ICP–MS. All TOC contents in the compilation were reported in previous studies. For samples with previously collected TOC data, the Re concentrations were measured on the same sample powders used for TOC determinations.

All datasets compiled from previous studies (tables S3 and S4 in the supplementary database) were filtered first to identify marine, fine-grained siliciclastic sediments based on literature information and petrographic examination. ORM are defined by having a total organic carbon

content of >0.4 wt% (Lyons and Severmann, 2006; Partin et al., 2013; Reinhard et al., 2013a), which also helps to avoid spuriously high Re/TOC ratios in our compilation. We further applied the geochemical filter of $Fe_T/Al > 0.5$, which typically delineates sediments deposited under anoxic conditions (e.g., Lyons and Severmann, 2006; Poulton et al., 2010; Planavsky et al., 2011). Where the above information is not available, efforts were made to determine local redox conditions using other geochemical proxies (e.g., Mo enrichments). We define Re concentrations equal to or greater than 5.0 ppb (i.e., >10 times the crustal average of ~0.2–0.4 ppb; Esser and Turekian, 1993; Peucker-Ehrenbrink and Jahn, 2001; Dubin and Peucker-Ehrenbrink, 2015) as being diagnostic for sediment anoxia. This approach enables an internally consistent compilation that includes samples deposited from weakly to mildly oxygenated waters (with sediment anoxia) and from fully anoxic waters. We assume that levels of authigenic Re enrichment in anoxic sediments generally scale to first-order with water column Re concentrations (i.e., following Algeo and Lyons, 2006 and Scott et al., 2008, for Mo), thus allowing us to track broad first-order changes in the Re concentration of ORM via comparison of time-bin averages. Although Re concentrations of less than 5.0 ppb may occur in some Archean ORM deposited beneath a fully anoxic atmosphere and oceans, only a minority of Archean samples had sufficiently low Re concentrations to be excluded from the compilation. We also note that Re concentrations in Unit I and II sediments of the restricted Black Sea are significantly above this threshold (~20–76 ppb; Ravizza et al., 1991; Crusius et al., 1996; Piper and Calvert, 2011); the filter therefore does not exclude Black Sea-type restricted basins from the compilation. As Re burial is independent of sulfide (H_2S) availability, no filter for euxinia is required as in the case for Mo. Temporal averages were binned at 5 Myr intervals ("time-point means") to compensate for age uncertainties; for example, the time-point mean $[Re]_{sed}$ for 660 Ma is the arithmetic mean of all

$[Re]_{sed}$ data from the ca. 657 Ma Aralka Formation (Schaefer and Burgess, 2003; Kendall et al., 2006) and the ca. 659 Ma Tashir Formation (Rooney et al., 2015).

Basin connectivity was inferred from sedimentology and paleogeographic reconstructions, where available. Because we model based on Re burial in unrestricted marine basins, we excluded units deposited in settings with obvious extreme basin restriction/isolation (i.e., terrestrial settings), where Re accumulation rates in sediments are typically lower compared with open-marine settings.

Published Re–Os depositional ages are listed in supplementary data tables (Table S4) to demonstrate minimal post-depositional disturbance of Re (cf. Anbar et al., 2007). Oxidative weathering is known to cause scatter in Re–Os isotope systematics in ORM (e.g., Georgiev et al., 2012); therefore, it is reasonable to expect that significantly later post-depositional penetration of O_2 would similarly disturb Re–Os systematics in ORM (Crusius and Thomson, 2003). ORM affected by post-depositional hydrothermal alteration, which is known to remobilize both elements, are excluded from the compilation (Kendall et al., 2009; Rooney et al., 2011). We included samples that have experienced anhydrous greenschist facies metamorphism because the Re–Os isotope systematics in ORM is not usually disturbed under such conditions (e.g., Kendall et al., 2004; Rooney et al., 2011).

Radioactive decay of ^{187}Re, which makes up ~63% of naturally occurring Re, causes the present-day Re concentration of ORM to be lower than that at the time of deposition. However, the slow rate of ^{187}Re decay (half-life = 41.6 Gyr) has a minimal effect on observed Re concentrations (maximum correction factor of ~3% for Archean ORM), and hence no correction was made for this effect.

4. Results

Our filtered compilation of $[Re]_{sed}$ (77 binned time points) and $[Re]_{sed}$/TOC (53 binned time points) through geologic time is presented in figures 1 and 2, with statistical parameters summarized in Table 4. The full compilation database is included as supplementary spreadsheet files (Tables S1–S2 for modern data and Tables S3–S5 for ancient data): all ancient $[Re]_{sed}$ and TOC data are reported in Table S3, with detailed unit descriptions and statistical summaries in Table S4. A salient observation of the compilation is that both $[Re]_{sed}$ and $[Re]_{sed}$/TOC display broad fluctuations through geologic time and that four distinct stages are discerned: 1) pre-GOE ($\geq$ 2.50 Ga), 2) the GOE, including the Lomagundi Event (2.50-2.05 Ga), 3) between the GOE and NOE (2.05-0.61 Ga), and 4) the NOE and Phanerozoic (0.61 Ga to present). For comparison, we calculated mean $[Re]_{sed}$ and $[Re]_{sed}$/TOC for the four stages by taking the arithmetic mean of the binned time-point means in each stage. Using the binned time-point means serves to minimize skewing of the stage mean values by individual ORM units with larger datasets. Mean $[Re]_{sed}$ for the four stages, calculated from time-point mean $[Re]_{sed}$ values (Table S4 in the supplementary database), are 13.0 ± 4.4 ppb (Stage 1; 1SD; 9 binned time points), 71.8 ± 44.8 ppb (Stage 2; 1SD; 3 binned time points), 20.8 ± 19.8 ppb (Stage 3; 1SD; 21 binned time points), and 154.9 ± 207.9 ppb (Stage 4; 1SD; 44 binned time points) (Table 4). Mean $[Re]_{sed}$/TOC for the four stages are 4.7 ± 2.7 ppb/wt.% (Stage 1; 1SD; 5 binned times points), 12.7 ± 5.8 ppb/wt.% (Stage 2; 1SD; 3 binned time points), 8.1 ± 3.5 ppb/wt.% (Stage 3; 1SD; 10 binned time points), and 31.3 ± 39.2 ppb/wt.% (Stage 4; 1SD; 35 binned time points). The time-point mean $[Re]_{sed}$ and $[Re]_{sed}$/TOC values at 1105 Ma (82.6 ppb, 16.0 ppb/wt.%) are significantly higher than the other stage 3 values, which range between 5.7 and 52.2 ppb and between 4.3 and 10.4 ppb/wt.%. If the 1105 Ma time-point mean is excluded, stage 3 has a mean $[Re]_{sed}$ of

17.7 ± 14.5 ppb (1SD; 20 binned time points) and a mean $[Re]_{sed}$/TOC of 7.3 ± 2.4 ppb/wt.% (1SD; 9 binned time points) (Table 4).

Because the time-binned mean $[Re]_{sed}$ and mean $[Re]_{sed}$/TOC in each stage do not follow a normal or log-normal distribution, bootstrap analysis was carried out to estimate the confidence interval of the binned time-point mean $[Re]_{sed}$ and mean $[Re]_{sed}$/TOC in stages 1, 3, and 4; stage 2 was excluded from bootstrap analysis due to the low number of time-point mean $[Re]_{sed}$ values (n=3) (see SI for details on the bootstrap analysis). The anomalous ca. 1105 Ma Touirist Formation is likewise excluded from stage 3 calculations (see section 5.1 for discussion). The means of 10,000 $[Re]_{sed}$ bootstrap time-point means (and associated 95% confidence intervals) for stages 1, 3, and 4 are 13 ppb (10, 17), 25 ppb (14, 37), and 151 ppb (95, 220), respectively (Table 4). The means of 10,000 $[Re]_{sed}$/TOC bootstrap time-point means (and associated 95% confidence intervals) for the same three stages are 5 ppb/wt.% (2, 7), 7 ppb/wt.% (5, 9), and 28 ppb/wt.% (18, 40), respectively (Table 4). A direct comparison of bootstrap statistics between stages 1, 3, and 4 shows that the bootstrap mean $[Re]_{sed}$ of stage 4 is distinct from the other two stages, with 95% confidence intervals taken into account; however, the bootstrap 95% confidence intervals for stages 1 and 3 overlap. The bootstrap analysis demonstrates that while high Re enrichment in stage 4 is statistically significant, the low $[Re]_{sed}$ values in stages 1 and 3 are statistically similar to each other.

Our plot of $[Re]_{sed}$ through time (Fig. 1) best shows the trend in maximum $[Re]_{sed}$ values, which to first-order reflects the maximum size of the Re seawater reservoir in each stage. The significance of the pattern displayed by the maximum $[Re]_{sed}$ trend is supported by mean $[Re]_{sed}$ values derived via bootstrap analysis (Table 4). The overall increase of Re concentrations in ORM across the Precambrian-Phanerozoic boundary is the most obvious feature of the Re

compilation. Our compilation suggests two separate stages of elevated $[Re]_{sed}$ during the latter part of the GOE (stage 2) and the Phanerozoic (stage 4), with the latter characterized by much higher maximum enrichments. Maximum $[Re]_{sed}$ in stages 1 and 3 (except the Touirist Formation) are lower by comparison, with stage 3 showing mildly higher values than stage 1. We further tested for possible bias of $[Re]_{sed}$ distribution by sample size. Median $[Re]_{sed}$ binned at 100 Myr intervals show only a very weak correlation with sample size ($R^2 = 0.03, n = 20, \rho = 0.48$; Fig. 3). We therefore consider it unlikely that the pattern of $[Re]_{sed}$ data is biased by sample size.

5. Discussion

5.1 Temporal trends in Re concentrations

Our temporal compilation of Re concentrations ($[Re]_{sed}$) in anoxic marine ORM (Fig. 1) displays four distinct stages that correspond to the evolution of atmospheric and oceanic O_2 content (Table 4). The choice of divisions is supported by statistical tests that confirm that the difference in average $[Re]_{sed}$ between stages is statistically significant (see section 4). We note that these first-order trends are still observed for a less rigorously filtered compilation. A similar trend is observed when Re concentrations are normalized to TOC contents (Fig. 2), demonstrating that the first-order secular variations in $[Re]_{sed}$, as represented by the four stages, likely result from first-order changes in the global seawater Re reservoir rather than changes in local organic carbon fluxes to the seafloor. Although variations in riverine Re fluxes might be linked to changes in crustal exhumation rates (e.g., during supercontinent assembly vs. dispersal) and a hypothesized transition from relatively more mafic to felsic continental crust by ca. 2.5 Ga (Dhuime et al., 2015; Tang et al., 2016; see Greber et al., 2017 for an alternative view arguing

for invariable composition of continental crust over the last ca. 3.5 Gyr), a simple sensitivity test of our mass-balance model demonstrates that such input flux variations should impart minimal influence on the $[Re]_{sed}$ record (SI). In general, our interpretation of atmosphere-ocean O_2 levels based on the Re record conforms well to that derived from the higher-resolution Cr and U records (Partin et al., 2013; Reinhard et al., 2013a).

Stage 1 covers the Archean ($\geq$ 2.50 Ga). Consistently low $[Re]_{sed}$ values during this interval indicates a small oceanic Re inventory, which in turn points to extensive seafloor anoxia and a small pre-GOE riverine Re flux because of an O_2-poor atmosphere. Some Late Archean units near the end of this stage have higher Re concentrations that are consistent with other geochemical evidence for transient increases in atmosphere-ocean O_2 levels that enabled oxidative dissolution of crustal sulfide minerals (Siebert et al., 2005; Anbar et al., 2007; Wille et al., 2007; Reinhard et al., 2009; Kendall et al., 2010, 2015a).

Stage 2 spans the time interval between 2.50 and 2.05 Ga and corresponds to an increase in global atmosphere-ocean O_2 content associated with the GOE (Bekker et al., 2004; Bekker and Holland, 2012; Planavsky et al., 2012; Partin et al., 2013). During the latter portion of the GOE, the ca. 2.22–2.06 Ga Lomagundi Event was likely marked by elevated organic matter burial as inferred from high $\delta^{13}C$ values in coeval carbonates. The high rates of primary productivity may have been driven by enhanced phosphorus fluxes to the oceans caused by the initial oxidative weathering of sulfide minerals in exposed Archean continental crust (Konhauser et al., 2011; Bekker and Holland, 2012). This organic matter burial event was likely accompanied by significant release of O_2 to the atmosphere (Karhu and Holland, 1996), consistent with geochemical and geological evidence for a shift to higher seawater concentrations of Mo, U, Cr, V, and SO_4^{2-} in response to this hypothesized increase in atmosphere-ocean oxygenation

(Schröder et al., 2008; Scott et al., 2008, 2014; Bekker and Holland, 2012; Planavsky et al., 2012; Reuschel et al., 2012; Sahoo et al., 2012; Partin et al., 2013; Reinhard et al., 2013a). As for other redox-sensitive metals, the increase in oxidative terrestrial weathering accompanying the GOE would have permanently established a continuous riverine flux of dissolved Re to the oceans that, along with contraction of seafloor anoxia, enabled buildup of a larger dissolved Re reservoir in oxygenated seawater. Such a scenario is supported by high average $[Re]_{sed}$ values for the Sengoma Argillite and Zaonezhskaya formations (117.4 and 87.1 ppb, respectively), which are well above the maximum average $[Re]_{sed}$ observed for any ORM in stage 1 (19.9 ppb).

There remains a general paucity of $[Re]_{sed}$ data from the early portion of stage 2 (between 2.5 and 2.1 Ga). The ca. 2.32 Ga Timeball Hill Formation displays $[Re]_{sed}$ values (average: 10.9 ppb) similar to stage 1 ORM (Diekrup, 2011). However, bottom water redox indicators (e.g., U and Mo enrichments and Fe speciation) suggest that the compiled Timeball Hill Formation analyses do not reflect strongly anoxic local water conditions (Diekrup, 2011) compared to other samples from the Timeball Hill Formation reported in the literature (e.g., Partin et al., 2013, and references therein). Future analyses of additional early stage 2 ORM, including other sections of the Timeball Hill Formation, are necessary to determine if higher $[Re]_{sed}$ values mark the onset of the GOE.

After the GOE, $[Re]_{sed}$ dropped significantly during stage 3 (2.05–0.61 Ga), approaching near-Archean values in many ORM. This decrease in authigenic Re enrichment mirrors a similar drop in the U, V, and Cr concentrations in ORM deposited over the one billion years after the Lomagundi Event (Sahoo et al., 2012; Partin et al., 2013; Reinhard et al., 2013a). Molybdenum abundances in stage 2 and 3 ORM, which are far more sensitive specifically to the extent of ocean euxinia rather than general anoxia compared with other redox-sensitive metals, are

intermediate between those seen in Archean and Phanerozoic ORM (Scott et al., 2008; Sahoo et al., 2012; Reinhard et al., 2013a). The lack of S-MIF in stage 3 sedimentary rocks indicates that atmospheric O_2 levels were high enough to support persistent oxidative mobilization of Re via weathering of crustal sulfide minerals and organic matter (Reinhard et al., 2013b; Planavsky et al., 2014; Greber et al., 2015; Cole et al., 2016). Hence, the drop in authigenic Re enrichments during stage 3 likely reflects an expansion of global ocean anoxia rather than a decline in the riverine Re flux. The $[Re]_{sed}$ in most stage 3 ORM are similar to stage 1 ORM, indicating that the extent of oxygenation generally remained far below that during the Lomagundi Event (stage 2), the latest Neoproterozoic, and the Phanerozoic (stage 4).

The ca. 1.1 Ga Touirist Formation, deposited in an epeiric sea during global sea-level high-stand (Gilleaudeau and Kah, 2015), has an average $[Re]_{sed}$ (82.6 ppb), which is significantly higher than the overall average of other stage 3 ORM (25.2 ppb) and is similar to stage 2 levels, suggesting that atmosphere-ocean oxygenation at ca. 1.1 Ga may have been higher than at other times during stage 3 after the Lomagundi Event. Some samples of the Touirist Formation have experienced contact metamorphism. However, the Re–Os isotope systematics of these thermally overmature samples is not significantly perturbed by flash pyrolysis, as indicated by a Re–Os age of 1105 ± 37 Ma (MSWD = 8.8) that, although exhibiting evidence for minor open-system behaviour (MSWD > 1), is not statistically different from a Re–Os age of 1107 ± 12 Ma (MSWD = 1.1) derived for a separate stratigraphic interval of thermally immature samples in the Touirist Formation (Rooney et al., 2010). Two samples with high Re concentrations of > 85 ppb come from the interval yielding a Re–Os isochron with MSWD of ~1, suggesting that the high Re levels in the Touirist Formation represent a primary sedimentary enrichment. Since a similar spike in sedimentary U enrichment is absent from the stage 3 records, including samples from

the same formation (Partin et al., 2013), a higher-resolution record of Re concentration for stage 3 is needed to robustly evaluate if the Touirist Formation truly represents an episode of higher oxygenation at ca. 1.1 Ga.

Stage 4 (<0.61 Ga) covers the latest Neoproterozoic, starting with the record of the NOE, and the Phanerozoic Eon. Along with high Mo, U, V, and Cr concentrations, the overall higher Re concentrations in ORM from this stage point to the build-up of dissolved, redox-sensitive trace metals in more oxygenated oceans (Scott et al., 2008; Sahoo et al., 2012; Partin et al., 2013; Reinhard et al., 2013a). Given the growing geochemical evidence for dynamic fluctuations in Neoproterozoic ocean redox conditions extending back to ca. 800 Ma (e.g., Sahoo et al., 2012, 2016; Planavsky et al., 2014; Kendall et al., 2015; Sperling et al., 2015; Thomson et al., 2015; Cole et al., 2016; Turner and Bekker, 2016; Kuznetsov et al., 2017), the boundary between stages 3 and 4 may potentially shift back in time with new Re data. We also note the general absence of high Re enrichments (like those observed in the Late Ediacaran, Early Cambrian (>535 Ma), and Late Phanerozoic ORM) during the early Paleozoic (535–375 Ma). Although the temporal resolution of the Re dataset is low for this time interval, the lower Re enrichments are consistent with less oxygenated conditions during the early Paleozoic compared with other Phanerozoic intervals. This inference is also consistent with generally lower U concentrations, lighter Mo isotope compositions, and Fe speciation evidence for widespread anoxic deposition of the Early Paleozoic ORM (Dahl et al., 2010; Partin et al., 2013; Sperling et al., 2015).

Following permanent establishment of widespread ocean oxygenation and contraction of anoxia to mostly marginal marine settings (i.e., oxygen-minimum zones and restricted basins), expansions of anoxia occurred as transient and sporadic oceanic anoxic events (OAEs), typically associated with mantle plume events, emplacement of Large Igneous Provinces (LIPs) and

submarine ocean plateaus, greenhouse conditions, extreme rates of continental weathering, and high pCO_2. During the Toarcian OAE, for example, the Re and Mo enrichments of ORM are muted, indicating drawdown of the oceanic Re and Mo reservoirs in response to expanded anoxia (Pearce et al., 2008; Owens et al., 2016). Conversely, during the Cretaceous OAEs 1a and 2, which were associated with LIP emplacement, Re concentrations of ORM are often not muted and are mildly correlated with excursions to higher Os concentrations and unradiogenic $^{187}Os/^{188}Os$, suggesting delivery of magmatic Re (and Os) to seawater in sufficient quantities to offset the increased burial of Re (and Os) into anoxic sediments (Turgeon and Creaser, 2008; Bottini et al., 2012; du Vivier et al., 2014; Kendall, 2014).

5.2 Constraints on the extent of mid-Proterozoic ocean anoxia

To arrive at a quantitative estimate for the extent of mid-Proterozoic ocean anoxia, we constructed a model relating seafloor redox distribution, Re burial rates under different redox regimes, and authigenic Re enrichment in anoxic sediments within a mass-balance framework built on observations from modern environments. Our model is adopted from that developed by Reinhard et al. (2013a) for the Cr and Mo records. A summary of the construction of the model is presented below, with details included in the SI.

We begin by defining the global Re marine reservoir in a conventional steady-state mass-balance, where the difference between mass entering (M_{in}) and exiting the system (M_{out}) equals change in storage:

$$M_{in} - M_{out} = \int_0^V [\mathrm{Re}]\, dV, \qquad \text{Eq. 1}$$

where dissolved Re concentration, [Re], is integrated over a global ocean volume, *V*. By taking the derivative with respect to time, *t*, the mass terms are replaced with source (F_{in}) and sink (F_{out}) fluxes:

$$F_{in} - F_{out} = \frac{d}{dt}\int_0^V [\mathrm{Re}]\, dV. \quad \text{Eq. 2}$$

As we are interested in long-term temporal shifts (>10^6 years) in ocean redox distribution, we assume steady-state conditions in the system ($\frac{d}{dt}\int_0^V [\mathrm{Re}]dV = 0$, and therefore $F_{in} = F_{out}$).

As outlined above, riverine delivery dominates the Re input flux to the oceans and is assumed to be constant for a post-GOE atmosphere-ocean system because atmosphere O_2 presumably remained high enough to support appreciable continental weathering/oxidation. Hydrothermal fluids, which are assumed to constitute a minor flux relative to riverine input in a post-GOE world (excluding transient magmatic-hydrothermal events), are excluded from consideration. Sink fluxes consist of Re removal to sediments under oxic, suboxic, and anoxic settings. Hence:

$$F_{in} = F_{oxic} + F_{suboxic} + F_{anoxic}. \quad \text{Eq. 3}$$

The sink terms are each expressed as:

$$F_i = \kappa A_i b_i, \quad \text{Eq. 4}$$

where A_i is the seafloor area covered by the specific redox setting (dimensions cm^2), and b_i is the characteristic metal burial rate for that setting as observed in the modern ocean (dimensions ng cm^{-2} y^{-1}). The non-dimensional coefficient κ relates Re burial flux to seawater concentration:

$$\kappa = \left(\frac{[\mathrm{Re}]'}{[\mathrm{Re}]_{\mathrm{M}}}\right)^{\alpha}, \quad \text{Eq. 5}$$

where $[\mathrm{Re}]'$ represents the seawater Re concentration under steady state in the investigated time interval, and $[\mathrm{Re}]_{\mathrm{M}}$ represents the modern seawater Re concentration. For a first-order mass-balance approach, α is set to unity to reflect the principle that, within a particular sink setting, the burial rate of a metal scales linearly with the size of its seawater reservoir (cf., Algeo and Lyons, 2006; Scott et al., 2008; Partin et al., 2013). Substitution and rearrangement of equations 3–5 yield a generalized expression for seawater Re concentration under new steady-state conditions following a perturbation to the global Re oceanic mass balance (cf., Reinhard et al., 2013a):

$$[\mathrm{Re}]' = [\mathrm{Re}]_{\mathrm{M}} \left(\frac{F_{in}}{\sum A_i b_i} \right), \qquad \text{Eq. 6}$$

where $[\mathrm{Re}]'$ varies as a function of A_i and b_i.

Authigenic Re enrichment in anoxic sediments under new steady-state conditions is governed by the general relationship:

$$b_a{}' = b_a \left(\frac{[\mathrm{Re}]'}{[\mathrm{Re}]_{\mathrm{M}}} \right), \qquad \text{Eq. 7}$$

where $b_a{}'$ is the anoxic burial rate under the new steady state, and b_a is the modern average anoxic burial rate. The anoxic burial rate at a specific point in time is a function of the magnitude of the marine Re reservoir, which in turn is controlled by the spatial distribution of the oxic, suboxic, and anoxic sinks (Eq. 6). To explore the marine Re cycle in ancient oceans, we apply a perturbation in the form of progressive expansion of anoxia, with predicted authigenic Re enrichment in open-ocean anoxic sediments, $[\mathrm{Re}]_{\mathrm{pred}}$, as the output.

A pitfall with previous attempts at modeling marine trace metal reservoirs is the assumption of a constant metal burial rate within a given sink—especially the anoxic sink—across the global seafloor. Essentially, a characteristic modern burial rate observed in anoxic basins is applied to the global seafloor, which is dominated by abyssal plains where overall sediment mass

accumulation rates are low. However, given that the fluxes of both detrital material and organic carbon decrease across the gradient from high-productivity margins to the open, deep-ocean floor, such an assumption results in unrealistically high sink fluxes for most deep sea anoxic sediments. This exaggeration leads to a model that is oversensitive to reducing conditions and thus underestimates the true extent of anoxia associated with a given inventory as recorded in the authigenic metal enrichment of anoxic ORM (e.g., Scott et al., 2008; Sahoo et al., 2012; Partin et al., 2013). Although this spatial dependence of metal burial rate is difficult to specify precisely in simple models and represents an important area of future work, we follow the approach of Reinhard et al. (2013a) by coupling a function that relates organic carbon flux to water depth with global bathymetric data (see SI for details). A tuneable burial rate ratio is then imposed to reproduce the characteristic modern Re anoxic burial rate (based on the Cariaco Basin data; see below and SI). These scaling factors are then incorporated into the general model equations (Eqs. 6 and 7) to calculate $[Re]_{pred}$ (see SI). As a significant improvement on the polynomial approximation used by Reinhard et al. (2013a) for relating carbon flux with bathymetry, we use bathymetric data from the eTOPO database (Amante and Eakins, 2009) and treat the bathymetric profile as a differentiable function to more accurately account for Re burial in shallow waters (see SI).

We adopted values from the well-characterized Cariaco Basin for our starting anoxic burial rate and bulk mass accumulation rate (BMAR; see SI). As the largest, relatively open-marine anoxic basin in the modern ocean, the Cariaco Basin best approximates the open-ocean conditions our model simulates (cf., Reinhard et al., 2013a). As mentioned earlier, anoxic Re burial rates in highly restricted basins (e.g., the Black Sea) are not appropriate because Re is strongly depleted from the water column under conditions of slow deep-water recharge

(Colodner et al., 1995). Because the Cariaco Basin has relatively high sedimentation and organic carbon burial rates compared with other modern anoxic basins and continental margin settings, we use the lowest BMAR of 0.01 g cm^{-2} yr^{-1} (with a factor of 1.5 above and below this value) from the range of published values for the Cariaco Basin (0.01–0.08 g cm^{-2} yr^{-1}; Calvert et al., 2015) to avoid overestimating Re burial flux for the anoxic sink (cf. Reinhard et al., 2013a). An ocean with BMAR values higher than the maximum value used for our model would be unrealistically efficient at removing Re to sediments and would yield an anomalously small extent of seafloor anoxia required to achieve the observed $[Re]_{sed}$.

The results of our mass-balance model are presented in Fig. 4. Overall, our model reveals that the marine Re reservoir is highly sensitive to the expansion of seafloor anoxia. The most dramatic drawdown in Re occurs with an expansion of anoxia from ~1% to ~10% of the modern seafloor area (Fig. 4), dominated by authigenic scavenging along relatively shallow productive marginal settings where organic carbon export to sediments is highest. At greater than 10% seafloor anoxia, the $[Re]_{pred}$ becomes significantly less sensitive to the extent of anoxia and decreases only slightly (by <10 ppb) between 10% and 100% of seafloor anoxia. This is due to the significantly lower burial rates for organic carbon over abyssal regions. Under conditions of complete seafloor anoxia, $[Re]_{pred}$ is 16–35 ppb for open-ocean ORM for the assumed range of BMAR. A model with a Re burial rate decoupled from spatial variations in organic carbon flux results in a steeper decrease of $[Re]_{pred}$ with increasing seafloor anoxia. In this case, significant underestimation of $[Re]_{pred}$ occurs past ~5% seafloor anoxia, at which point anoxia expands beyond the ocean margins into the open ocean where rates of primary productivity and organic carbon burial are much lower than at the margins.

The uncertainty regarding mid-Proterozoic bathymetry is a challenge for our model. In particular, epeiric seas are virtually absent today but were more prevalent during at least some time intervals in the Precambrian and Phanerozoic (Eriksson et al., 1998). To evaluate the effect of epeiric seas, we repeated our model exercise and simulated epeiric sea expansion by applying prescribed sea-level rise to modern ocean bathymetry (Fig. 5; SI). In this scenario, Re drawdown is enhanced by elevated burial with organic-rich sediments underlying more extensive productive shallow waters. The net effect of epeiric sea expansion is a reduction in the predicted extent of seafloor anoxia required to achieve the same value of $[Re]_{pred}$ when modeled with only limited extent of epeiric seas.

To allow robust comparison of the model's $[Re]_{pred}$ for anoxic ORM with the mid-Proterozoic record, we took a conservative approach using ORM with arguably the best independent constraints on local redox conditions. Specifically, we calculated the mean $[Re]_{sed}$ values for those stage 3 ORM that have independent Fe speciation evidence for deposition from anoxic bottom waters—specifically ratios of biogeochemically highly reactive Fe to total Fe (Fe_{HR}/Fe_T) greater than 0.38 or degree-of-pyritization (DOP) values greater than 0.45 (Table S5 in the supplementary database; Raiswell and Canfield, 1998; Poulton and Raiswell, 2002; reviewed in Lyons and Severmann, 2006). These filters should largely exclude any ORM deposited under suboxic bottom waters. Based on the observed Re enrichments in independently constrained mid-Proterozoic anoxic ORM, we can infer the extent of seafloor anoxia using the model. For comparison, we performed the same exercise for the anoxic ORM from stages 1 and 2.

Based on comparison with the model, the five ORM units from stage 3 with Fe speciation data reveal a range of ocean redox states based on Re enrichments (Table 5). The ca. 1417 Ma

Lower Velkerri Formation and ca. 1050 Ma Bylot Supergroup are characterized by low average $[Re]_{sed}$ values that imply near-total seafloor anoxia for the entire range of assumed BMAR (except for an oxygenated surface layer in contact with the mildly oxygenated post-GOE atmosphere). In detail, however, the average $[Re]_{sed}$ values for these units are lower than those predicted by the model for total seafloor anoxia (Fig. 4), suggesting that partial basin restriction, a greater extent of epeiric seas during their deposition relative to today, and/or an unusually low local BMAR is a factor. The Re data from the ca. 1825 Ma Rove Formation are also consistent with a significant extent of ocean anoxia except at the lowermost end of the modeled range of BMAR. Similarly, Re data for Archean ORM predominantly require extensive ocean anoxia for most of the assumed range of BMAR. In contrast, the ca. 2105 Ma Sengoma Argillite Formation and the ca. 2050 Ma Zaonezhskaya Formation from late stage 2 are characterized by high average $[Re]_{sed}$, suggesting that <3% of the seafloor was covered by anoxic waters, consistent with a greater extent of ocean oxygenation during the GOE.

Despite the complications posed by partial basin restriction and development of epeiric seas on the magnitude of Re enrichment in some ORM, the stage 3 ORM in our full compilation show Re enrichments that are generally similar to or only mildly higher than those of the stage 1 ORM from the predominantly anoxic Archean. This observation, independent of the model constraints, points to generally low O_2 concentrations in post-GOE oceans prior to stage 4. Whereas muted Re enrichment in stage 1 reflects predominant marine anoxia and a low riverine input due to low atmospheric O_2 levels, muted Re enrichment in stage 3 is a product of substantial drawdown fluxes despite an appreciable input flux. A similar line of reasoning was invoked to explain the nearly similar U concentrations in Archean and mid-Proterozoic ORM (Partin et al., 2013), and both records are consistent with interpretations based on the records for Cr enrichment (Reinhard

et al., 2013a) and isotopic trends (Planavsky et al., 2014; Cole et al., 2016). However, as stressed by Partin et al. (2013), Cole et al. (2016), and Reinhard et al. (2016), such an interpretation is only meant to represent the first-order marine redox landscape and does not preclude the possibility of spatiotemporal variations in atmosphere-ocean redox during mid-Proterozoic time.

Indeed, the higher average $[Re]_{sed}$ values from the ca. 1361 Ma Upper Velkerri Formation and ca. 641 Ma Black River Dolomite yield estimates of only 2–13% and 1–4% seafloor anoxia, respectively, suggesting that a larger oceanic Re reservoir and thus a greater extent of ocean oxygenation may have existed during these intervals, albeit not all comparable to Phanerozoic levels. Consistent with this interpretation, U isotope data from the same samples of the Upper Velkerri Formation suggest that <25% of the seafloor was covered by anoxic waters (Yang et al., 2017). Our interpretation is also consistent with Mo concentration and isotope data for these ORM (Kendall et al., 2009, 2015b), which constrain the extent of ocean euxinia rather than general ocean anoxia (euxinic plus ferruginous conditions). The model does not preclude the possibility that a significant portion of the low-productivity regions of the deep oceans may have been covered by weakly oxygenated waters (Slack et al., 2007, 2009), nor does it preclude oxygenated surface waters in highly productive regions (Sperling et al., 2014; Reinhard et al., 2016).

Rhenium enrichments in the Black River Dolomite are consistent with increased ocean oxygenation in the wake of the Sturtian glaciation, as suggested by Planavsky et al. (2010). While Re data from the upper Velkerri and Touirist formations may potentially reflect transiently oxygenated marine conditions, the extent to which these data represent spatiotemporal variations in the mid-Proterozoic atmosphere-ocean redox state remains to be tested with higher-resolution Re data for stage 3. Given recent trace element evidence for fluctuating redox conditions in the

Neoproterozoic (e.g., Sahoo et al., 2012, 2016; Planavsky et al., 2014; Kendall et al., 2015; Sperling et al., 2015; Thomson et al., 2015; Cole et al., 2016), transient episodes of broader ocean oxygenation in the Mesoproterozoic may be part of a dynamic, longer-term trend of protracted oxygenation—one characterized by significant temporal oscillations in atmosphere-ocean O_2 levels likely around still low baselines, which extended into the Neoproterozoic and early Paleozoic.

6. Conclusions

The redox-sensitive behaviour of Re can be used to characterize the evolution of ancient marine redox conditions by examining the sedimentary enrichment of Re in ORM through geologic time. A salient feature of our $[Re]_{sed}$ compilation is significantly lower Re concentrations in mid-Proterozoic ORM compared to many ORM deposited during the ca. 2.22–2.06 Ga Lomagundi Event and during the Phanerozoic Eon. Rhenium enrichments these mid-Proterozoic ORM are overall only mildly higher than those of Archean ORM. Given that efficient oxidative mobilization of Re from sulfide minerals and organic matter in the exposed upper continental crust was established and sustained since the GOE, the muted Re enrichments in mid-Proterozoic ORM are consistent with an expansion of global marine anoxia after ca. 2.05 Ga that led to significant drawdown of the seawater Re inventory. This conclusion is further supported by mass-balance modeling of the marine Re geochemical cycle, which indicates that low Re enrichments in some mid-Proterozoic ORM are consistent with extensive seafloor anoxia. In this respect, the Re compilation agrees with previous Cr, Mo, and U evidence for pervasively anoxic and ferruginous conditions in mid-Proterozoic oceans. The distinctive sensitivity of Re to varying environmental controls allows additional capacity to resolve spatiotemporal patterns in

the ancient redox landscape. This is evidenced in a subset of the mid-Proterozoic ORM which displays higher Re enrichments that may reflect transient episodes of ocean oxygenation. The extent to which these data represent spatiotemporal variations in the mid-Proterozoic atmosphere-ocean redox state, the duration of these variations, and the possibility of other such events remains to be tested with an improved understanding of the modern oceanic Re cycle and a higher temporal resolution for the Re compilation.

Acknowledgements

This project was supported by the Natural Sciences and Engineering Research Council of Canada (NSERC) Discovery Grant Program and Accelerator Grants, NSERC USRA, the NASA Astrobiology Institute, the Agouron Institute, and the NSF Earth-Life Transitions and FESD programs. Xinze Lu provided guidance for bootstrap analysis.

References

Algeo T.J. and Lyons T.W. (2006) Mo–total organic carbon covariation in modern anoxic marine environments: Implications for analysis of paleoredox and paleohydrographic conditions. *Paleoceanography* **21**, PA1016.

Amante C. and Eakins B.W. (2009) ETOPO1 1 arc-minute global relief model [electronic resource]: procedures, data sources and analysis. NOAA Technical Memorandum NESDIS NGDC-24. U.S. Dept. of Commerce, National Oceanic and Atmospheric Administration, National Environmental Satellite, Data, and Information Service, National Geophysical Data Center, Marine Geology and Geophysics Division, Boulder, CO. Accessed November 20, 2014.

Anbar A.D., Creaser R.A., Papanastassiou D.A. and Wasserburg G.J. (1992) Rhenium in seawater: Confirmation of generally conservative behavior. *Geochim. Cosmochim. Acta* **56**, 4099–4103.

Anbar A.D., Duan Y., Lyons T.W., Arnold G L., Kendall B., Creaser R.A., Kaufman A.J., Gordon G. W., Scott C., Garvin J. and Buick R. (2007) A whiff of oxygen before the Great Oxidation Event? *Science* **317**, 1903–1906.

Bekker A. (2014) Great Oxygenation Event, In Encyclopedia of Astrobiology (eds. R. Amils, M. Gargaud, J.C. Quintanilla, H.J. Cleaves, W.M. Irvine, D. Pinti and M. Viso). Springer-Verlag, New York. pp. 1–9.

Bekker A. and Holland H.D. (2012) Oxygen overshoot and recovery during the early Paleoproterozoic. *Earth Planet. Sci. Lett.* **317**–**318**, 295–304.

Bekker A., Holland H.D., Wang P., Rumble D., Stein H.J., Hannah J.L., Coetzee L.L. and Beukes N.J. (2004) Dating the rise of atmospheric oxygen. *Nature* **427**, 117–120.

Bekker A., Slack J.F., Planavsky N., Krapež B., Hofmann A., Konhauser K.O. and Rouxel O.J. (2010) Iron Formation: The Sedimentary Product of a Complex Interplay among Mantle, Tectonic, Oceanic, and Biospheric Processes. *Econ. Geol.* **105**, 467–508.

Bekker A., Planavsky N., Krapež B., Rasmussen B., Hofmann A., Slack J.F., Rouxel O.J. and Konhauser K.O. (2013) Iron Formations: Their Origins and Implications for Ancient Seawater Chemistry. In *Treatise on Geochemistry* (eds. H. Holland and K. Turekian). Elsevier, Amsterdam. pp. 561–628.

Bottini C., Cohen A. S., Erba E., Jenkyns H. C. and Coe A. L. (2012) Osmium-isotope evidence for volcanism, weathering, and ocean mixing during the early Aptian OAE 1a. *Geology* **40**, 583–586.

Calvert S. E., Piper D. Z., Thunell R. C. and Astor Y. (2015) Elemental settling and burial fluxes in the Cariaco Basin. *Mar. Chem.* **177**, 607–629.

Cohen A. S., Coe A. L., Bartlett J. M. and Hawkesworth C. J. (1999) Precise Re–Os ages of organic-rich mudrocks and the Os isotope composition of Jurassic seawater. *Earth Planet. Sci. Lett.* **167**, 159–173.

Cole D.B., Reinhard C.T., Wang X., Gueguen B., Halverson G.P., Gibson T., Hodgkiss M.S.W., McKenzie N.Y., Lyons T.W. and Planavsky N.J. (2016) A shale-hosted Cr isotope record of low atmospheric oxygen during the Proterozoic. *Geology* **44**, 555–558.

Colodner D. (1991) The marine geochemistry of rhenium, iridium and platinum. Ph. D. thesis. Massachusetts Institute of Technology, 269 pp.

Colodner D., Sachs J., Ravizza G., Turekian K., Edmond J. and Boyle E. (1993) The geochemical cycle of rhenium: a reconnaissance. *Earth Planet. Sci. Lett.* **117**, 205–221.

Colodner D., Edmond J. and Boyle E. (1995) Rhenium in the Black Sea: comparison with molybdenum and uranium. *Earth Planet. Sci. Lett.* **131**, 1–15.

Crusius J. and Thomson J. (2003) Mobility of authigenic rhenium, silver, and selenium during postdepositional oxidation in marine sediments. *Geochim. Cosmochim. Acta* **67**, 265–273.

Crusius J., Calvert S., Pedersen T. and Sage D. (1996) Rhenium and molybdenum enrichments in sediments as indicators of oxic, suboxic and sulfidic conditions of deposition. *Earth Planet. Sci. Lett.* **145**, 65–78.

Dahl T.W., Hammarlund E.U., Anbar A.D., Bond D.P.G., Gill B.C., Gordon G.W., Knoll A.H., Nielsen A.T., Schovsbo N.H. and Canfield D.E. (2010) Devonian rise in atmospheric oxygen correlated to the radiations of terrestrial plants and large predatory fish. *Proc. Natl. Acad. Sci. U.S.A.* **107**, 17911–17915.

Daines S.J., Mills B.J.W. and Lenton T.M. (2017) Atmospheric oxygen regulation at low Proterozoic levels by incomplete oxidative weathering of sedimentary organic carbon. *Nature Commun.* **8**, 14379.

Dalai T.K., Suzuki K., Minagawa M., Nozaki Y. (2005) Variations in seawater osmium isotope composition since the last glacial maximum: A case study from the Japan Sea. *Chem. Geol.* **220**, 303–314.

Davis J.D. (1984) Western Cape Cod Bay: Hydrographic, Geological, Ecological, and Meteorological Backgrounds for Environmental Studies. In *Observations on the Ecology and Biology of Western Cape Cod Bay, Massachusetts* (eds. J.D. Davis and D. Merriman) Springer-Verlag, New York. 18 pp.

Dhuime B., Wuestefeld A. and Hawkesworth C. J. (2015) Emergence of modern continental crust about 3 billion years ago. *Nat. Geosci.* **8**, 552–555.

Diekrup, D. (2011) Early Paleoproterozoic oceanic redox conditions and metabolic pathways revealed by C, S, Fe, and trace metal geochemistry. MSc thesis. Institut für Geologie und Paläontologie Westfälische Wilhelms-Universität Münster, Münster, Germany. 43 pp.

Du Vivier A.D.C., Selby D., Sageman B.B., Jarvis I., Gröcke D.R. and Voigt S. (2014) Marine $^{187}Os/^{188}Os$ isotope stratigraphy reveals the interaction of volcanism and ocean circulation during Oceanic Anoxic Event 2. *Earth Planet. Sci. Lett.* **389**, 23–33.

Dubin A. and Peucker-Ehrenbrink B. (2015) The importance of organic-rich shales to the geochemical cycles of rhenium and osmium. *Chem. Geol.* **403**, 111–120.

Dufour R. and Quellet P. (2007) *Estuary and Gulf of St. Lawrence marine ecosystem overview and assessment report.* Fisheries and Oceans Canada, Ottawa. 112 pp.

Eriksson P.G., Condie K.C., Tirsgaard H., Mueller W.U., Altermann W., Miall A.D., Aspler L.B., Catuneanu O. and Chiarenzelli J.R. (1998) Precambrian clastic sedimentation systems. *Sediment. Geol.* **120**, 5–53.

Esser B.K. and Turekain K.K. (1993) The osmium isotopic composition of the continental crust. *Geochim. Cosmochim. Acta* **57**, 3093–3104.

Farquhar J., Bao H. and Thiemens M. (2000) Atmospheric influence of Earth's earliest sulfur cycle. *Science* **289**, 756–758.

Frei R., Gaucher C., Poulton S.W. and Canfield D.E. (2009) Fluctuations in Precambrian atmospheric oxygenation recorded by chromium isotopes. *Nature* **461**, 250–253.

Georgiev S., Stein H.J., Hannah J.L., Weiss H.M., Bingen B., Xu G., Rein E., Hatlø V., Løseth H., Nali M. and Piasecki S. (2012) Chemical signals for oxidative weathering predict Re–Os isochroneity in black shales, East Greenland. *Chem. Geol.; Special Issue Recent Advances in Trace Metal Applications to Paleoceanographic Studies* **324–325**, 108–121.

Gilleaudeau, G.J. and Kah L.C. (2015) Heterogeneous redox conditions and a shallow chemocline in the Mesoproterozoic ocean: Evidence from carbon–sulfur–iron relationships. *Precambrian Res.* **257**, 94–108.

Gilleaudeau G.J., Frei R., Kaufman,A.J., Kah,L.C., Azmy K., Barley J.K., Chernyavskiy P. and Knoll, A.H. (2016) Oxygenation of the mid-Proterozoic atmosphere: clues from chromium isotopes in carbonates. *Geochem. Perspect. Lett.* **2**, 178–187.

Greber N.D., Mäder U. and Nägler T.F. (2015) Experimental dissolution of molybdenum-sulphides at low oxygen concentrations: A first-order approximation of late Archean atmospheric conditions. *Earth Space Sci.* **2**, 173–180.

Greber N.D., Dauphas N., Bekker A., Ptáček M.P., Bindeman I.N. and Hofmann A. (2017) Titanium isotopic evidence for felsic crust and plate tectonics 3.5 billion years ago. *Science* **357**, 1271–1274.

Gumsley A.P., Chamberlain K.R., Bleeker W., Söderlund U., de Kock M.O., Larsson E.R. and Bekker A. (2017) Timing and tempo of the Great Oxidation Event. *Proc. Natl. Acad. Sci. U.S.A.* **114**, 1811–1816.

Hannah J.L., Bekker A., Stein H.J., Markey R.J. and Holland H.D. (2004) Primitive Os and 2316 Ma age for marine shale: implications for Paleoproterozoic glacial events and the rise of atmospheric oxygen. *Earth Planet. Sci. Lett.* **225**, 43–52.

Hardisty D.S., Lu Z.-l., Bekker A., Diamond C.W., Gill B.C., Jiang G.-q., Kah L.C., Knoll A.H., Loyd S.J. and Osburn M.R. (2017) Perspectives on Proterozoic surface ocean redox from iodine contents in ancient and recent carbonate. *Earth Planet. Sci. Lett.* **463**, 159–170.

Hay B.J. (1988) Sediment accumulation in the central western Black Sea over the past 5100 years. *Paleoceanogr.* **3**, 491–508

Hay B.J., Arthur M.A., Dean W.E., Neff E.D. and Honjo S. (1991) Sediment deposition in the late Holocene abyssal Black Sea: With climatic and chronologic implications. *Deep Sea Res. Part A* **38**, S1211–1235.

Hazen R.M., Bekker A., Bish D.L., Bleeker W., Downs R.T., Farquhar J., Ferry J.M., Grew E.S., Knoll A.H., Papineau D., Ralph J.P., Sverjensky D.A. and Valley J.W. (2011) Needs and opportunities in mineral evolution research. *Am. Mineral.* **96**, 953–963.

Helz G.R. and Dolor M.K. (2012) What regulates rhenium deposition in euxinic basins? *Chem. Geol.* **304–305**, 131–141.

Iwanowicz H.R., Anderson R.D., Ketschke B.A. (1973) *A study of the marine resources of Hingham Bay*. Mass. Division of Marine Fisheries. 40 pp.

Karhu J.A. and Holland H.D. (1996) Carbon isotopes and the rise of atmospheric oxygen. *Geology* **24**, 867–870.

Kendall B. (2014) An osmium-based method for assessing the source of dissolved rhenium and molybdenum to Archean seawater. *Chem. Geol.* **385**, 92–103.

Kendall B., Creaser R. A., Ross G. M. and Selby D. (2004) Constraints on the timing of Marinoan "Snowball Earth" glaciation by ^{187}Re-^{187}Os dating of a Neoproterozoic, post-glacial black shale in Western Canada. *Earth Planet. Sci. Lett.* **222**, 729–740.

Kendall B., Creaser R. A. and Selby D. (2006) Re-Os geochronology of postglacial black shales in Australia: Constraints on the timing of "Sturtian" glaciation. *Geology* **34**, 729-732.

Kendall B., Creaser R.A., Gordon G.W. and Anbar A.D. (2009) Re–Os and Mo isotope systematics of black shales from the Middle Proterozoic Velkerri and Wollogorang Formations, McArthur Basin, northern Australia. *Geochim. Cosmochim. Acta* **73**, 2534–2558.

Kendall B., Reinhard C.T., Lyons T.W., Kaufman A.J., Poulton S.W. and Anbar A.D. (2010) Pervasive oxygenation along late Archaean ocean margins. *Nat. Geosci.* **3**, 647–652.

Kendall B., Creaser R.A., Reinhard C.T., Lyons T.W. and Anbar A.D. (2015a) Transient episodes of mild environmental oxygenation and oxidative continental weathering during the Late Archean. *Sci. Adv.* **1**: e1500777.

Kendall B., Komiya T., Lyons T.W., Bates S.M., Gordon G.W., Romaniello S.J., Jiang G., Creaser R.A., Xiao S., McFadden K., Sawaki Y., Tahata M., Shu D., Han J., Li Y., Chu X. and Anbar A.D. (2015b) Uranium and molybdenum isotope evidence for an episode of widespread ocean oxygenation during the late Ediacaran Period. *Geochim. Cosmochim. Acta* **156**, 173–193.

Koide M., Hodge V F., Yang J.S., Stallard M., Goldberg E.G., Calhoun J. and Bertine K.K. (1986) Some comparative marine chemistries of rhenium, gold, silver and molybdenum. *Appl.Geochem.* **1**, 705–714.

Konhauser K.O., Lalonde S.V., Planavsky N.J., Pecoits E., Lyons T.W., Mojzsis S.J., Rouxel O.J., Barley M.E., Rosìere C., Fralick P.W., Kump L.R. and Bekker A. (2011) aerobic pyrite oxidation and acid rock drainage during the Great Oxidation Event. *Nature* **478**, 369–373.

Kump L.R., Junium C., Arthur M.A., Brasier A., Fallick A., Melezhik V., Lepland A., Črne A.E. and Luo G. (2011) Isotopic evidence for massive oxidation of organic matter following the Great Oxidation Event. *Science* **334**, 1694–1696.

Kuznetsov A.B., Bekker A., Ovchinnikova G.V., Gorokhov I.M. and Vasilyeva I.M. (2017) Unradiogenic strontium and moderate-amplitude carbon isotope variations in early

Tonian seawater after the assembly of Rodinia and before the Bitter Springs Excursion, *Precambrian Res.*, in press. https://doi.org/10.1016/j.precamres.2017.06.011

Liu X.-M., Kah L.C., Knoll A.H., Kaufman A.J., Shahar A. and Hazen R.M. (2016) Tracing Earth's O_2 evolution using Zn/Fe ratios in marine carbonates. *Geochem. Perspect. Lett.* **2**, 24–34.

Lyons T.W. and Severmann S. (2006) A critical look at iron paleoredox proxies: new insights from modern euxinic marine basins. *Geochim. Cosmochim. Acta* **70**, 5698–5722.

Lyons T.W., Reinhard C.T. and Planavsky N.J. (2014) The rise of oxygen in Earth's early ocean and atmosphere. *Nature* **506**, 307–315.

McKay J.L., Pedersen T.F., Mucci A. (2007) Sedimentary redox conditions in continental margin sediments (N.E. Pacific) — Influence on the accumulation of redox-sensitive trace metals. *Chem. Geol.* **238**, 180–196.

McLennan S.M. (2001) Relationships between the trace element composition of sedimentary rocks and upper continental crust. *Geochem. Geophys. Geosyst.* **2**, 1021.

Miller C.A., Peucker-Ehrenbrink B., Walker B.D. and Marcantonio F. (2011) Re-assessing the surface cycling of molybdenum and rhenium. *Geochim. Cosmochim. Acta* **75**, 7146–7179.

Moore T.C. and the Expedition 302 Scientists (2006) Sedimentation and subsidence history of the Lomonosov Ridge. In: Backman J., Moran K., McInroy D.B., Mayer L.A., and the Expedition 302 Scientists (eds), *Proc. IODP 302*. Integrated Ocean Drilling Program Management International, Inc., Edinburgh. 7 pp.

Morford J.L. and Emerson S. (1999) The geochemistry of redox sensitive trace metals in sediments. *Geochim. Cosmochim. Acta* **63**, 1735–1750.

Morford J.L., Emerson S.R., Breckel E.J. and Kim S.H. (2005) Diagenesis of oxyanions (V, U, Re, and Mo) in pore waters and sediments from a continental margin. *Geochim. Cosmochim. Acta* **69**, 5021–5032.

Morford J.L., Martin W.R., Kalnejais L. H., François R., Bothner M. and Karle I.-M. (2007) Insights on geochemical cycling of U, Re and Mo from seasonal sampling in Boston Harbor, Massachusetts, USA. *Geochim. Cosmochim. Acta* **71**, 895–917.

Morford J.L., Martin W.R. and Carney C.M. (2012) Rhenium geochemical cycling: Insights from continental margins. *Chem. Geol.* **324–325**, 73–86.

Mukherjee I. and Large R.R. (2016) Pyrite trace element chemistry of the Velkerri Formation, Roper Group, McArthur Basin: Evidence for atmospheric oxygenation during the Boring Billion. *Precambrian Res.* **281**, 13–26.

Naqvi W. (1991) Geographical extent of denitrification in the Arabian Sea in relation to some physical processes. *Oceanolog. Acta.* **14**, 281–290.

O'Regan M. (2007) Data report: high-resolution bulk density, dry density, and porosity records from the Arctic Coring Expedition, IODP Expedition 302. In Backman J., Moran K., McInroy D.B., Mayer L.A., and the Expedition 302 Scientists (eds.), *Proc. IODP 302*. Integrated Ocean Drilling Program Management International, Inc., Edinburgh. 15 pp.

Owens J.D., Reinhard C.T., Rohrssen M., Love G.D. and Lyons T.W. (2016) Empirical links between trace metal cycling and marine microbial ecology during a large perturbation to Earth's carbon cycle. *Earth Planet. Sci. Lett.* **449**, 407–417.

Partin C.A., Bekker A., Planavsky N.J., Scott C.T., Gill B.C., Li C., Podkovyrov V., Maslov A., Konhauser K.O., Lalonde S.V., Love G.D., Poulton S.W. and Lyons T. W. (2013) Large-

scale fluctuations in Precambrian atmospheric and oceanic oxygen levels from the record of U in shales. *Earth Planet. Sci. Lett.* **369–370**, 284–293.

Pavlov A.A. and Kasting J.F. (2002) Mass-independent fractionation sulfur isotopes in Archean sediments: strong evidence for an anoxic Archean atmosphere. *Astrobiology* **2**, 27–41.

Pearce C.R., Cohen A.S., Coe A.L. and Burton K.W. (2008) Molybdenum isotope evidence for global ocean anoxia coupled with perturbations to the carbon cycle during the Early Jurassic. *Geology* **36**, 231–234.

Peterson L.C., Haug G.H., Murray R.W., Yarincik K.M., King J.W., Bralower T.J., Kameo K., Rutherford S.D. and Pearce R.B. (2000) Late Quaternary stratigraphy and sedimentation at Site 1002, Cariaco Basin (Venezuela). In Leckie, R.M., Sigurdsson, H., Acton, G.D. and Draper, G. (Eds.), *Proc. IODP* **165**, 85–99.

Peucker-Ehrenbrink B. and Jahn B.-M. (2001) Rhenium-osmium isotope systematics and platinum group element concentrations: Leoss and the upper continental crust. *Geochem. Geophys. Geosyst.* **2**, 2001GC000172.

Piper D. Z. and Calvert S. E. (2011) Holocene and late glacial palaeoceanography and palaeolimnology of the Black Sea: Changing sediment provenance and basin hydrography over the past 20,000 years. *Geochim. Cosmochim. Acta.* **75**, 5597-5624.

Planavsky N.J., Rouxel O.J., Bekker A., Lalonde S.V., Konhauser K.O., Reinhard C.T. and Lyons T.W. (2010) The evolution of the marine phosphate reservoir. *Nature* **467**, 1088–1090.

Planavsky N.J., McGoldrick P., Scott C.T., Li C., Reinhard C.T., Kelly A.E., Chu X., Bekker A., Love G.D. and Lyons T.W. (2011) Widespread iron-rich conditions in the mid-Proterozoic ocean. *Nature* **477**, 448–451.

Planavsky N.J., Bekker A., Hofmann A., Owens J.D. and Lyons T.W. (2012) Sulfur record of rising and falling marine oxygen and sulfate levels during the Lomagundi event. *Proc. Natl. Acad. Sci. U.S.A.* **109**, 18300–18305.

Planavsky N.J., Reinhard C.T., Wang X., Thomson D., McGoldrick P., Rainbird R.H., Johnson T., Fischer W.W. and Lyons T.W. (2014) Low Mid-Proterozoic atmospheric oxygen levels and the delayed rise of animals. *Science* **346**, 635–638.

Planavsky N.J., Cole D.B., Reinhard C.T., Diamond C., Love G.D., Luo G., Zhang S., Konhauser K.O. and Lyons T.W. (2016) No evidence for high atmospheric oxygen levels 1,400 million years ago. *Proc. Natl. Acad. Sci. U.S.A.* **113**, 2550–2551.

Poirier A. (2006) Re–Os and Pb isotope systematics in reduced fjord sediments from Saanich Inlet (Western Canada). *Earth Planet. Sci. Lett.* **249**, 119–131.

Poirier A. and Hillaire-Marcel C. (2011) Improved Os-isotope stratigraphy of the Arctic Ocean. *Geophys. Res. Lett.* **38**, L14607.

Poulton S.W. and Raiswell R. (2002) The low-temperature geochemical cycle of iron: From continental fluxes to marine sediment deposition. *Am. J. Sci.* **302**, 774–805.

Poulton S.W., Fralick P.W. and Canfield D.E. (2010) Spatial variability in oceanic redox structure 1.8 billion years ago. *Nat. Geosci.* **3**, 486–490.

Raiswell R. and Canfield D. E. (1998) Sources of iron for pyrite formation in marine sediments. *Am. J. Sci.* **298**, 219–245.

Ravizza G., Turekian K. K. and Hay B. J. (1991) The geochemistry of rhenium and osmium in recent sediments from the Black Sea. *Geochim. Cosmochim. Acta.* **55**, 3741-3752.

Reimers C.E., Ruttenberg K.C., Canfield D.E., Christiansen M.B., Martin J.B. (1996) Porewater pH and authigenic phases formed in the uppermost sediments of the Santa Barbara Basin. *Geochim. Cosmochim. Acta.* **60**, 4037–4057.

Reinhard C.T., Raiswell R., Scott C., Anbar A.D. and Lyons T.W. (2009) A late Archean sulfidic sea stimulated by early oxidative weathering of the continents. *Science* **326**, 713–716.

Reinhard C.T., Planavsky N.J., Robbins L.J., Partin C.A., Gill B.C., Lalonde S.V., Bekker A., Konhauser K.O. and Lyons T.W. (2013a) Proterozoic ocean redox and biogeochemical stasis. *Proc. Natl. Acad. Sci. U.S.A.* **110**, 5357–5362.

Reinhard C.T., Lalonde S.V. and Lyons T.W. (2013b) Oxidative sulfide dissolution on the early Earth. *Chem. Geol.* **362**, 44–55.

Reinhard C.T., Planavsky N.J., Olson S.L., Lyons T.W. and Erwin D.H. (2016) Earth's oxygen cycle and the evolution of animal life. *Proc. Natl. Acad. Sci. U.S.A.* **113**, 8933–8938.

Reuschel M., Melezhik V.A., Whitehouse M.J., Lepland A., Fallick A.E. and Strauss H. (2012) Isotopic evidence for a sizeable seawater sulfate reservoir at 2.1 Ga. *Precambrian Res.* **192–195**, 78–88.

Rooney A.D., Chew D.M. and Selby D. (2011) Re–Os geochronology of the Neoproterozoic–Cambrian Dalradian Supergroup of Scotland and Ireland: Implications for Neoproterozoic stratigraphy, glaciations and Re–Os systematics. *Precambrian Res.* **185**, 202–214.

Rooney A.D., Selby D., Houzay J. and Renne P.R. (2010) Re–Os geochronology of a Mesoproterozoic sedimentary succession, Taoudeni basin, Mauritania: Implications for basin-wide correlations and Re–Os organic-rich sediments systematics. *Earth Planet. Sci. Lett.* **289**, 486–496.

Rooney A. D., Strauss J. V., Brandon A. D. and Macdonald F. A. (2015) A Cryogenian chronology: Two long-lasting synchronous Neoproterozoic glaciations. *Geology* **43**, 459-462.

Sahoo S.K., Planavsky N.J., Kendall B., Wang X., Shi X., Scott C., Anbar A.D., Lyons T. W. and Jiang G. (2012) Ocean oxygenation in the wake of the Marinoan glaciation. *Nature* **489**, 546–549.

Sahoo S.K., Planavsky N.J., Jiang G., Kendall B., Owens J.D., Wang X., Shi X., Anbar A.D. and Lyons, T.W. (2016) Ocean oxygenation events in the anoxic Ediacaran ocean. *Geobiology* **14**, 457–468.

Schaefer B. F. and Burgess J. M. (2003) Re–Os isotopic age constraints on deposition in the Neoproterozoic Amadeus Basin: implications for the 'Snowball Earth'. *J. Geol. Soc. London* **160**, 825-828.

Schröder S., Bekker A., Beukes N.J., Strauss H. and Van Niekerk H.S. (2008) Rise in seawater sulphate concentration associated with the Paleoproterozoic positive carbon isotope excursion: evidence from sulphate evaporites in the ~2.2–2.1 Gyr shallow-marine Lucknow Formation, South Africa. *Terra Nova* **20**, 108–117.

Scott C. and Lyons T.W. (2012) Contrasting molybdenum cycling and isotopic properties in euxinic versus non-euxinic sediments and sedimentary rocks: Refining the paleoproxies. *Chem. Geol.* **324–325**, 19–27.

Scott C., Lyons T.W., Bekker A., Shen Y., Poulton S.W., Chu X. and Anbar A.D. (2008) Tracing the stepwise oxygenation of the Proterozoic ocean. *Nature* **452**, 456–459.

Scott C., Planavsky N.J., Dupont C.L., Kendall B., Gill B.C., Robbing L.J., Husband K.F., Arnold G.L., Wing B.A., Bekker A., Anbar A.D., Konhauser K.O. and Lyons T.W. (2013) Bioavailability of zinc in marine systems through time. *Nat. Geosci.* **6**, 125–168.

Scott C., Wing B.A., Bekker A., Planavsky N.J., Medvedev P., Bates S.M., Yun M. and Lyons T.W. (2014) Pyrite multiple-sulfur isotope evidence for rapid expansion and contraction of the early Paleoproterozoic seawater sulfate reservoir. *Earth Planet. Sci. Lett.* **389**, 95–104.

Selby D. and Creaser R.A. (2003) Re–Os geochronology of organic rich sediments: an evaluation of organic matter analysis methods. *Chem. Geol.* **200**, 225–240.

Siebert C., Kramers J.D., Meisel T., Morel P. and Nägler T.F. (2005) PGE, Re–Os, and Mo isotope systematics in Archean and early Proterozoic sedimentary systems as proxies for redox conditions of the early Earth. *Geochim. Cosmochim. Acta* **69**, 1787–1801.

Slack J.F., Grenne T., Bekker A., Rouxel O.J. and Lingberg P.A. (2007) Suboxic deep seawater in the late Paleoproterozoic: Evidence from hematitic chert and iron formation related to seafloor-hydrothermal sulfide deposits, central Arizona, USA. *Earth Planet. Sci. Lett.* **255**, 243–256.

Slack J.F., Grenne T. and Bekker A. (2009) Seafloor-hydrothermal Si–Fe–Mn exhalites in the Pecos greenstone belt, New Mexico, and the redox state of ca. 1720 Ma deep seawater. *Geosphere* **5**, 302–314.

Sperling E.A., Rooney A.D., Hays L., Sergeev V.N., Vorob'eva N.G., Sergeeva N.D., Selby D., Johnston D.T. and Knoll A.H. (2014) Redox heterogeneity of subsurface waters in the Mesoproterozoic ocean. *Geobiology* **12,** 373–386.

Sperling E.A., Wolock C.J., Morgan A.S., Gill B.C., Kunzmann M., Halverson G.P., Macdonald F.A., Knoll A.H. and Johnston D.A. (2015) Statistical analysis of iron geochemical data suggests limited late Proterozoic oxygenation. *Nature* **523**, 451–454.

Sundby B., Martinez P. and Gobeil C. (2004) Comparative geochemistry of cadmium, rhenium, uranium, and molybdenum in continental margin sediments. *Geochim. Cosmochimi. Acta.* **68**, 2485–2493.

Sverdrup H.U., Johnson M.W. and Fleming R.H. (1942) *The oceans: their physics, chemistry, and general biology*. Prentice-Hall, New York.

Sverjensky D.A. and Lee N. (2010) The Great Oxidation Event and mineral diversification. *Elements* **6**, 31–36.

Tang D., Shi X., Wang X. and Jiang G. (2016) Extremely low oxygen concentration in mid-Proterozoic shallow seawaters. *Precambrian Res.* **276**, 145–157.

Thomson D., Rainbird R., Planavsky N., Lyons T.W. and Bekker A. (2015) Chemostratigraphy of the Shaler Supergroup, Victoria Island, NW Canada: A record of ocean composition prior to the Cryogenian glaciations. *Precambrian Res.* **263**, 232–245.

Tribovillard N., Algeo T.J., Lyons T. and Riboulleau A. (2006) Trace metals as paleoredox and paleoproductivity proxies: An update. *Chem. Geol.* **232**, 12–32.

Turner E.C. and Bekker A. (2016) Thick sulfate evaporite accumulations marking a mid-Neoproterozoic oxygenation event (Ten Stone Formation, Northwest Territories, Canada), *GSA Bulletin* **128**, 203–222.

van der Weijden C.H., Reichart G. And van Os B. J. H., 2006. Sedimentary trace element records over the last 200 kyr from within and below the northern Arabian Sea oxygen minimum zone. *Mar. Geol.* **231**, 69–88.

Wille M., Kramers J.D., Nägler T.F., Beukes N.J., Schröder S., Meisel T., Lacassie J.P. and Voegelin A.R. (2007) Evidence for a gradual rise of oxygen between 2.6 and 2.5 Ga from Mo isotopes and Re-PGE signatures in shales. *Geochim. Cosmochim. Acta* **71**, 2417–2435.

Wollast R. (2002) Continental Margins - Review of Geochemical Settings. In *Ocean Margin Systems* (eds. G. Wefer, D. Billett, D. Hebbeln, B.B. Jørgensen, M. Schlüter and T.C.E. van Weering). Springer-Verlag, Berlin Heidelberg. pp. 15–31.

Xiong Y. and Wood S.A. (2002) Experimental determination of the hydrothermal solubility of ReS_2 and the Re–ReO_2 buffer assemblage and transport of rhenium under supercritical conditions. *Geochem. Trans.* **3**, 1.

Xiong Y. and Wood S.A. (1999) Experimental determination of the solubility of ReO_2 and the dominant oxidation state of rhenium in hydrothermal solutions. *Chem. Geol.* **158**, 245–256.

Yang G., Hannah J.L., Zimmerman A., Stein H.J. and Bekker A. (2009) Re–Os depositional age for Archean carbonaceous slates from the southwestern Superior Province: challenges and insights. *Earth Planet. Sci. Lett.* **280**, 83–92.

Yang S., Kendall B., Lu X., Zhang F. and Zheng W. (2017) Uranium isotope compositions of Mid-Proterozoic black shales: evidence for an episode of increased ocean oxygenation at 1.36 Ga and evaluation of the effect of post-depositional hydrothermal fluid flow. *Precambrian Res.* **298**, 187-201.

Zbinden E.A., Holland H.D., Feakes C.R. and Dobos S.K. (1988) The Sturgeon Falls paleosol and the composition of the atmosphere 1.1 Ga BP. *Precambrian Res.* **42**, 141–163.

Zhang S., Wang X., Wang H., Bjerrum C.J., Hammarlund E.U., Costa M.M., Connelly J.N., Zhang B., Su J. and Canfield D.E. (2016) Sufficient oxygen for animal respiration 1,400 million years ago. *Proc. Natl. Acad. Sci. U.S.A.* **113**, 1731–1736.

Table 1. Comparison of Re, Cr and U enrichment levels in modern anoxic marine sediments.

Element	Upper Crust Concentration[1]	Average Conc.[1] In Modern[2] Anoxic Marine Sediments	Enrichment Factor[3]
Re	0.2–0.4	65.5	218
Cr	85	94.6	1.1
U	2.8	11.1	4.0

[1] Re in ppb; Cr and U in ppm

[2] Modern data defined as datasets with an age younger than 1 Ma

[3] Enrichment factor = anoxic sediment conc. / upper crust conc.

Re data: Esser and Turekian (1993); Peucker-Ehrenbrink and Jahn (2001); Dubin and Peucker-Ehrenbrink (2015); this study (see supplementary spreadsheet files, Tables S1–S2)

Cr data: McLennan (2001); Reinhard et al. (2013a)

U data: McLennan (2001); Partin et al. (2013)

Table 2. Re burial rates in modern marine sediments. Basin mass accumulation rates are listed for anoxic sediments only. Oxygen penetration depth is given for suboxic and oxic sediments where available. Italicized names under the "Sampled Sediments" column are sub-basins within the same margin (in bold) and from which an arithmetic average is taken to represent the overall margin burial rate. Only center-justified values under the "Re Burial Rate" column are used in calculating weighted averages. This is done for the suboxic and oxic sinks; the modern anoxic sink burial rate is calculated from Cariaco Basin data (Supplementary information).

Sampled Sediments	Redox State	O_2 Penetration Depth (cm)	Basin MAR ($g\ cm^{-2}yr^{-1}$)	Re Burial Rate ($ng\ cm^{-2}yr^{-1}$)	Areal Extent (cm^2)	Weighing Factor	Representative Sink Re Burial Rate, b_i ($ng\ cm^{-2}yr^{-1}$)	References
OXIC								
Pelagic Sediments	oxic			1.2×10^{-5} [a]	2.7×10^{18} [b]	78.4%	1.6×10^{-3}	Colodner (1991)
Oxic Continetal Margins				7.4×10^{-3}	7.4×10^{17} [c]	21.6%		
Sea of Japan	oxic to suboxic			*1.1×10^{-4}*				Crusius et al. (1996); Dalai et al. (2005)
Lomonosov Ridge	oxic			*4.3×10^{-4}* [d]				Poirier & Hillaire-Marcel (2011)
NW US Margin, St 6, 8	oxic	1.5-5		*1.4×10^{-3}*				Morford et al. (2005)
African Margin, 2BC, 3BC	oxic	>3		*2.8×10^{-2}*				Morford and Emerson (1999); Morford et al. (2005)
SUBOXIC							0.41	
African Margin, 1BC	suboxic	0.9		0.42	8.0×10^{14} [e]	4.1%		Morford and Emerson (1999); Morford et al. (2005)
Laurentian Trough	suboxic	0.4-0.8		0.33	2.4×10^{15} [f]	12.4%		Sundby et al. (2004)
Buzzards Bay	suboxic	0.25-0.85		0.56	6.2×10^{12} [g]	0.03%		Morford et al. (2009)
Hingham Bay	suboxic	0.2-0.6		1.04	3.4×10^{11} [h]	0.002%		Morford et al. (2009)
Gulf of California				1.45	8.0×10^{14}	4.1%		Colodner et al. (1993)
Carmen	suboxic			*1.4*				Colodner et al. (1993)
San Pedro Matir	suboxic			*1.5*				Colodner et al. (1993)
Californian Borderlands				0.855	8.0×10^{14}	4.1%		Colodner et al. (1993)
Santa Barbara	suboxic	0-0.5 [i]		*0.7*				Colodner et al. (1993)
San Clemente	suboxic	0.4		*0.55*				Morford et al. (2005)
San Nicolas	suboxic	0.1		*1.4*				Morford et al. (2005)
Santa Cruz	suboxic	0.1		*0.77*				Morford et al. (2005)
W. American Margin				0.19	8.0×10^{14} [e]	4.1%		
NW US Margin, St 2, 4	suboxic	0.3-0.5		*0.24*				Morford et al. (2005)
NW US Margin, WEC	suboxic	0.3-0.9		*0.3*				Morford and Emerson (1999); Morford et al. (2005)
Western Canadian Margin	oxic to suboxic	0.4-0.7		*0.029*				McKay et al. (2007)
Arabian Sea					1.4×10^{16} [j]	71%		
Murray Ridge, PC463	suboxic			0.36				van der Weijden et al. (2006)
ANOXIC								
Cariaco Basin	anoxic			1.34-1.56			1.34	Calvert et al. (2015), new data
Walvis Bay	anoxic		0.11	2.1				Colodner et al. (1993)
Saanich Inlet	seasonally anoxic		0.616	1-1.5				Poirier (2006)
Chile Shelf	anoxic		0.033	3.2				Colodner et al. (1993)
Peru Shelf	intermittently anoxic; upwelling zone		0.0242	0.5				Colodner et al. (1993)
Black Sea	anoxic; restricted		0.0055-0.0078	0.15-0.54				Hay (1988), Hay et al. (1991), Ravizza et al. (1991)

a. Calculated from data of North Atlantic sediments; a value of 1.2×10^{-5} ng $cm^{-2}yr^{-1}$ is chosen. Observed range is 2×10^{-6}–2×10^{-4} ng $cm^{-2}yr^{-1}$
b. Sverdrup et al. (1942)
c. Wollast (2003)
d. Calculated from sedimentation rate and dry bulk density data from Moore et al. (2006) and O'Regan (2007), respectively.
e. Area assumed to be the same as Californian Borderlands
f. Dufour and Ouellet (2007)
g. Davis (1984)
h. Iwanowicz et al. (1973)
i. Reimers et al. (1996)
j. Area affected by denitrification only; Naqvi (1991)

Table 3. Parameters of modern marine Re sink fluxes (see Table 2 for comprehensive literature data used for estimating b_i.)

	% Area Seafloor, k_i	Characteristic Burial Rate, b_i (ng/cm^2/yr)	Sink Flux, F_{out} (mol/yr)	% of Input Flux
Oxic	83.89%	1.60×10^{-3}	2.61×10^{4}	6.08%
Suboxic	4.67%	4.15×10^{-1}	3.75×10^{5}	87.41%
Anoxic	0.11%	1.339	2.80×10^{4}	6.52%

Table 4. Average $[Re]_{sed}$, $[Re]_{sed}$/TOC ratio, and associated standard deviation (1σ) for each stage. To calculate statistical values for each stage, arithmetic mean values were first calculated for each 5 Ma binned interval (time-point means; table S4 in the supplementary database). Stage mean values, bootstrap mean values, and bootstrap 95% confidence intervals were then calculated from these time-point means (see section 4.1). Bootstrap analysis was not performed for stage 2 due to low number of time-binned data (n=2). The anomalous ~1.1 Ga Touirist Formation is excluded from stage 3 calculations.

Stage	Age Interval (Ga)	$[Re]_{sed}$ n*	Mean $[Re]_{sed}$ (ppb)	Bootstrap mean $[Re]_{sed}$ (ppb)	Bootstrap 95% confidence interval	$[Re]_{sed}$ /TOC n*	Mean $[Re]_{sed}$ / TOC (ppb/wt%)	Bootstrap mean $[Re]_{sed}$ / TOC (ppb/wt%)	Bootstrap 95% confidence interval
1	2.72–2.50	9	13	13	10–17	5	5	5	2–7
2	2.50–2.05	3	72	–	–	3	13	–	–
3	2.05–0.61	20	18	25	14–37	9	7	7	5–9
4	0.61–0.00	44	155	151	95–220	35	31	28	18–40

* "n" here denotes the number of time-point means under each stage (table S4 in the supplementary database).

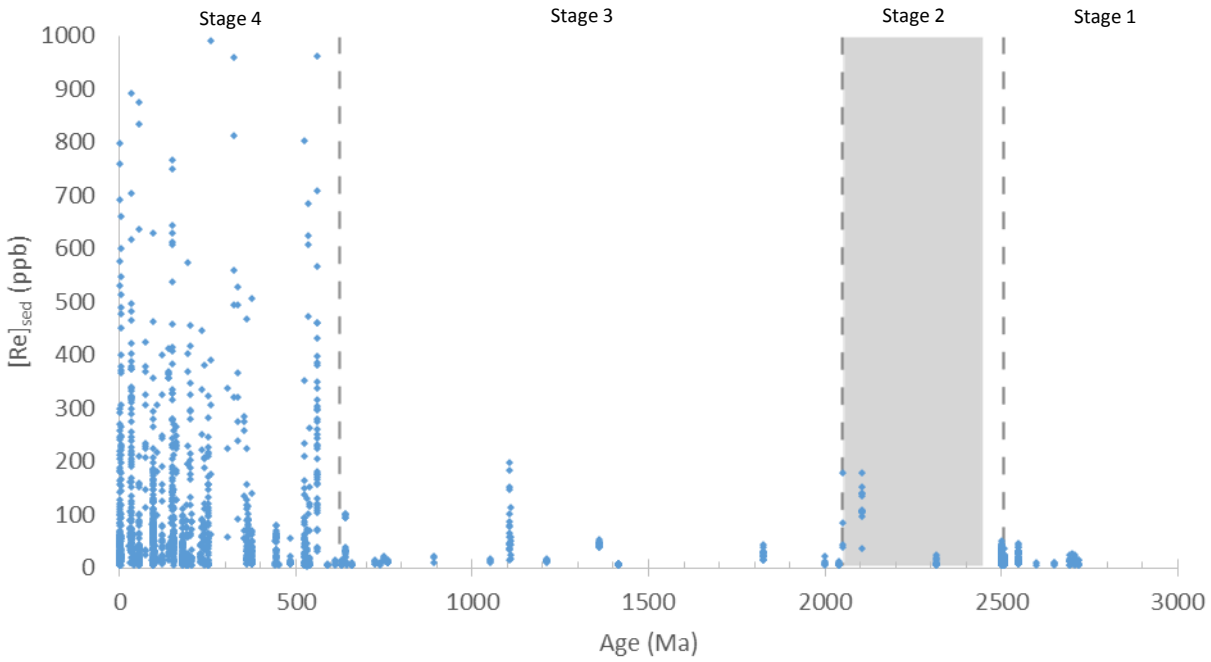

Figure 1. Re concentrations in anoxic, marine organic-rich mudrocks through time (n = 1,771; filtered). Phanerozoic values above 1000 ppb (n = 15) are not displayed. Shaded grey bar represents approximate span of the Great Oxidation Event (GOE).

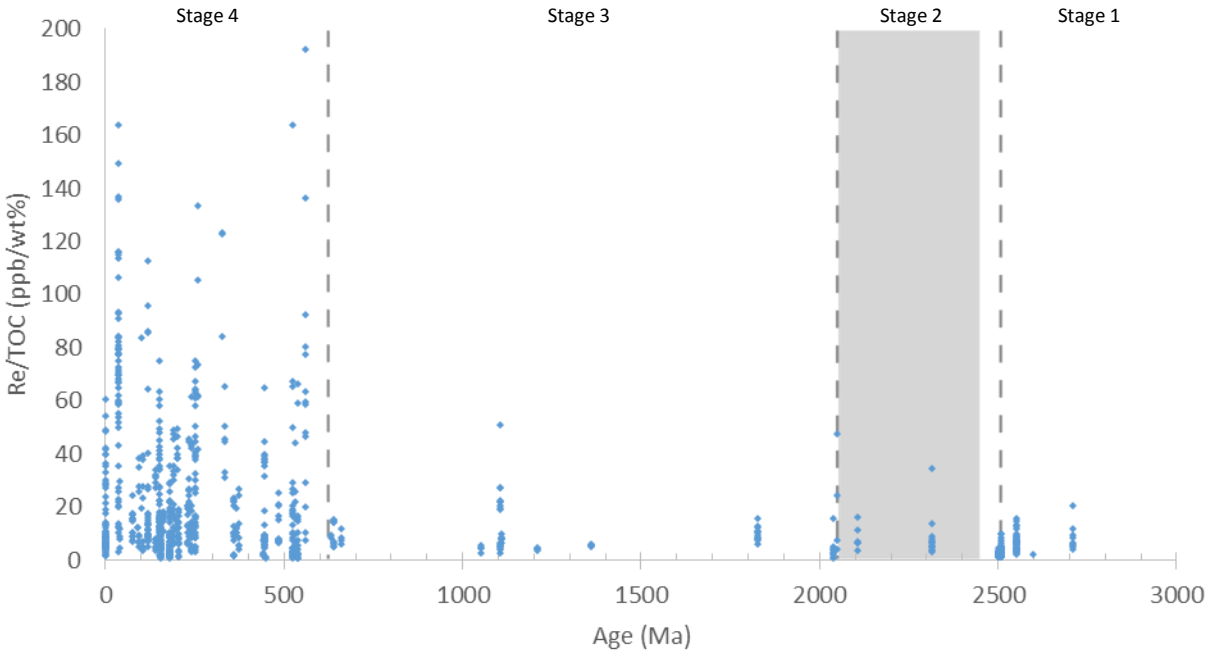

Figure 2. Re concentration normalized to total organic carbon content (TOC) through time (n = 977). Phanerozoic values above 200 ppb/wt% (n = 8) are not displayed.

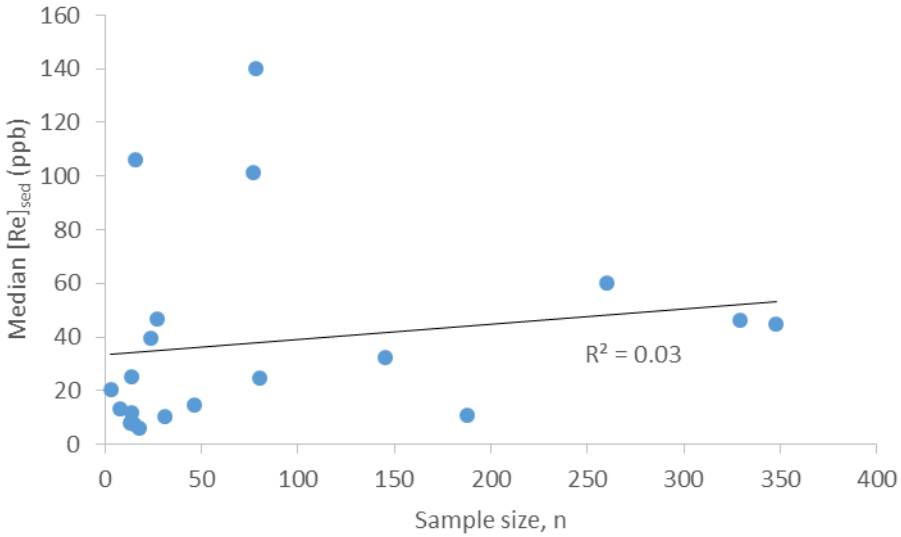

Figure 3. Sample size plotted against median $[Re]_{sed}$ with 100 Myr bins. Sample size and median $[Re]_{sed}$ are not well-correlated (R^2 = 0.03, n = 20, ρ = 0.48).

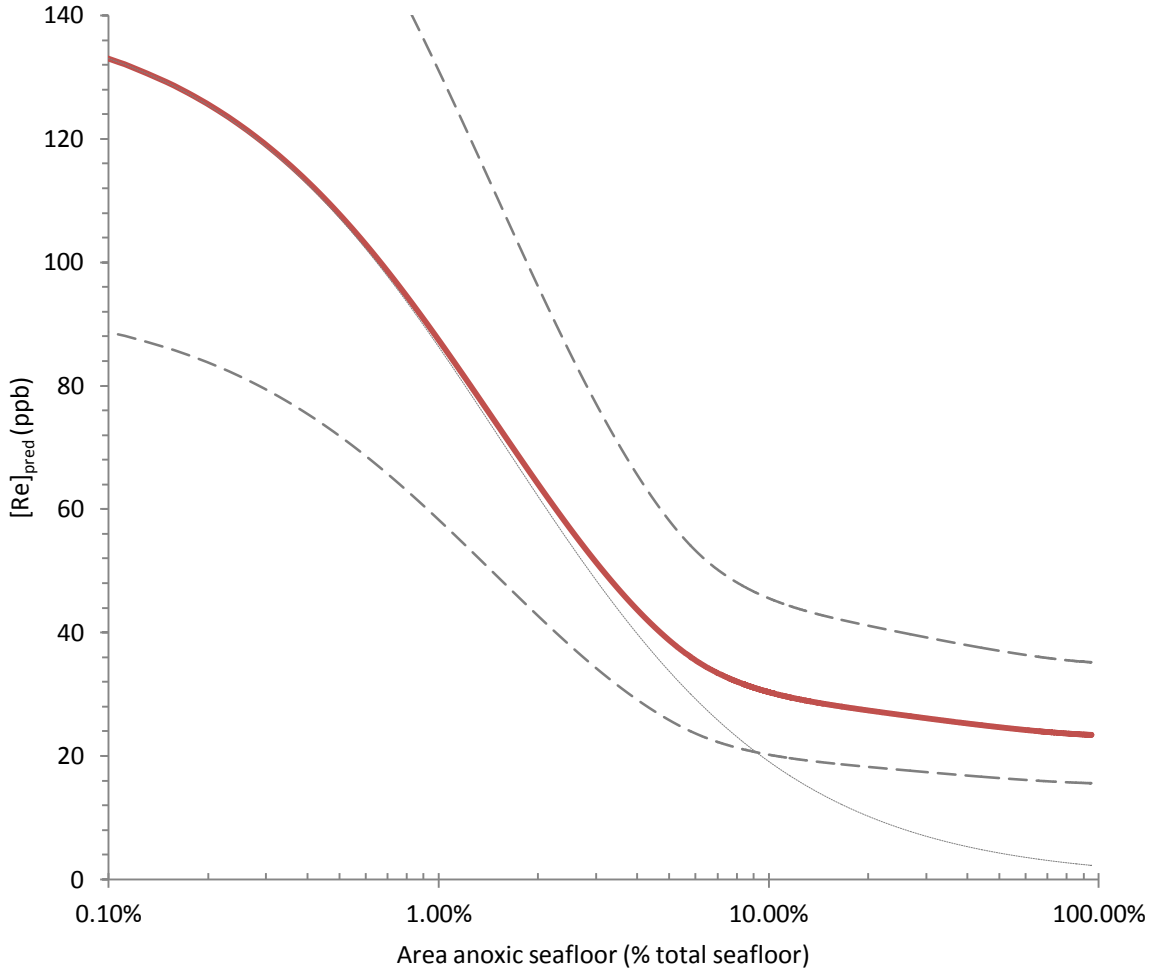

Figure 4. Modeled authigenic Re abundances in anoxic organic-rich mudrocks, $[Re]_{pred}$, versus prescribed extent of anoxia expansion (red curve). Dashed curves represent a factor of 1.5 above and below a bulk mass accumulation rate of 0.01 g $cm^{-2}yr^{-1}$, constrained from the Cariaco Basin. A model assuming a spatially invariant metal burial rate (dotted curve) underestimates the extent of seafloor anoxia for a given $[Re]_{pred}$.

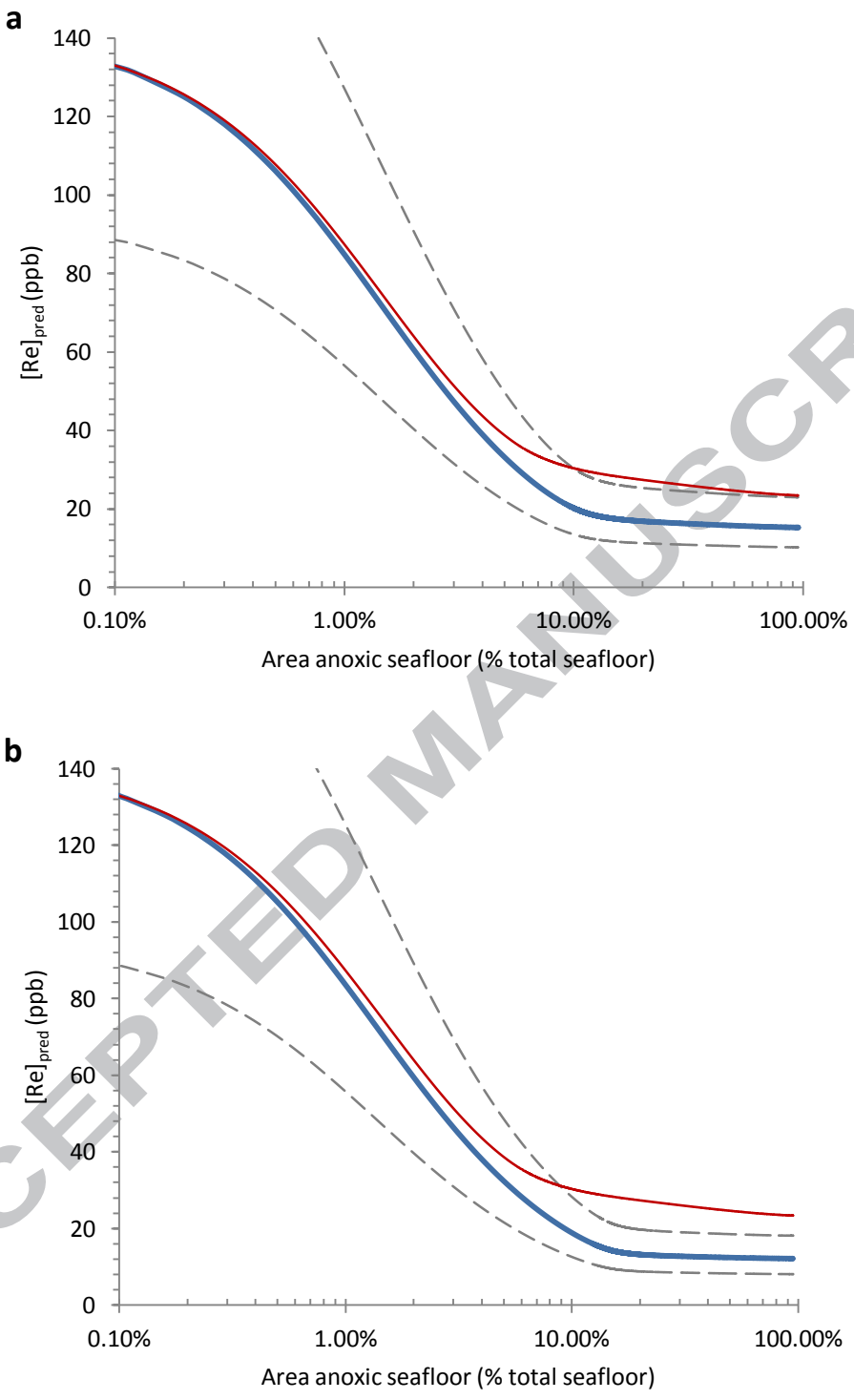

Figure 5. Modeled $[Re]_{pred}$ (blue curve) for an expansion of epeiric seas resulting from a) a 100 m sea level rise, and b) a 200 m sea level rise. Dashed curves represent factor of 1.5 above and below a bulk mass accumulation rate of 0.01 g $cm^{-2}yr^{-1}$. Modeled $[Re]_{pred}$ without epeiric expansion is shown as the red curve for comparison.

Table 5. Mean $[Re]_{sed}$, $[Re]_{sed}$/TOC ratio, and model estimates for the extent of seafloor anoxia of >590 Ma ORM deposited under anoxic bottom water conditions as constrained by $Fe_{HR}/Fe_T > 0.38$ or DOP > 0.45. For each interval, estimates of seafloor anoxia is given for model runs with three different BMAR values (see footnote). Data sources are listed in supplementary data tables.

Stage	Unit Name	Compilation age (Ma)	n	Mean $[Re]_{sed}$ (ppb)	n	Mean $[Re]_{sed}$/TOC (ppb/wt%)	Extent of seafloor anoxia (% seafloor area)		
							Max. BMAR[1]	Mean BMAR[2]	Min. BMAR[3]
1	Carajas Formation	2710	5	12.3	5	7.6	100%	100%	100%
	Upper Nauga Formation	2550	4	22.3	4	6.6	7%	100%	100%
	Klein Naute Formation	2510	30	13.5	30	3.0	100%	100%	100%
	Mt. McRae Shale	2500	28	25.1	24	2.4	5%	43%	100%
2	Timeball Hill Formation	2315	3	14.3	3	6.1	100%	100%	100%
	Sengoma Argillite Formation	2105	6	114.4	6	8.6	0%	0%	1%
	Zaonezhskaya Formation	2050	1	85.3	1	47.4	0%	1%	3%
3	Rove Formation	1825	11	26.6	11	10.2	5%	26%	100%
	Lower Velkerri Formation	1415	1	5.8	–	–	100%	100%	100%
	Upper Velkerri Formation	1360	6	44.2	6	5.7	2%	4%	13%
	Arctic Bay, Victoria Bay, Athole Point Formations	1050	2	13.9	2	3.8	100%	100%	100%
	Black River Dolomite	640	10	65.0	10	10.4	1%	2%	4%

[1] Maximum BMAR = 0.01 g cm^{-2} yr^{-1} × 1.5

[2] Mean BMAR = 0.01 g cm^{-2} yr^{-1}

[3] Minimum BMAR = 0.01 g cm^{-2} yr^{-1} / 1.5